

**Evolution of Cranial Morphology and the Functional Consequences of Echolocation
in Bats**

Delaney Gilley

A Thesis Presented to the Graduate Faculty of Middle Tennessee State University in
Partial Fulfillment of the Requirements for the Degree of Master of Science in Biology

Middle Tennessee State University

December 2022

Thesis Committee:

Dr. Jessica Arbour, Chair

Dr. Sarah Bergemann

Dr. Brian Miller

ACKNOWLEDGEMENTS

Words cannot express my gratitude to my supervisor, Dr. Jessica Arbour, for her invaluable patience and feedback. I could not have completed this journey without her continuous support and guidance to help me conquer any challenges from my research. She has helped me mature, not only as a professional scholar and researcher but also, as an individual. It would not have been possible to accomplish all I have done without her generous help.

I am deeply grateful for my committee members, Dr. Brian Miller and Dr. Sarah Bergemann for their support and encouragement. Their advice and inspirations have helped me stay confident in my research and have allowed my thesis and research project to be successful.

I would like to thank all my peers, especially Lexi Hamous and Dan Bryant who have aided me through much need advice, editing help, and moral support throughout my entire degree.

Finally, I would like to thank my family for their love and support throughout my entire life. Above all I would like to thank my husband, Jacob Gilley, for endless support, constant reassurance and, overall, being with me every step of this journey. Final thanks to Roxie and Remus Gilley for providing comfort and unlimited support.

ABSTRACT

Chiroptera (bats) is the second most species-rich mammalian order and has extraordinary diversity in cranial shape and function. This diversity includes three echolocation modalities and numerous dietary specializations, which have been linked to ecological, behavioral, and sensory adaptations. Previous analyses have suggested that the positioning of the rostrum relative to the basicranium (upturned or downturned snout) is linked to the evolution of echolocation modes. I tested this hypothesis directly by quantifying rostral flexion via 3D geometric morphometrics and using phylogenetic comparative methods to detect macroevolutionary patterns across 235 species of bats. I found that >30% of variation in skull shape is linked to rostral flexion. Disparity through time analysis indicates that the rostral angle of modern lineages was established early in the evolution of most clades, and that echolocation modes have different adaptive optima. Finally, I analyzed biomechanical consequences associated with extreme upturned rostra. I found that unilateral bites have an increase of stress associated with a decrease in rostral flexion (upturned snout) then an increase in flexion (downturned rostrum). This provides evidence for variation in dietary opportunity between different echolocating groups. Overall, I find that rostral flexion is a key element of cranial diversity of bats that played a strong role early in the adaptation of this trait and has broad ranging consequences for the biomechanical properties of the skull. Evolution to different echolocation modes likely significantly constrained subsequent diversification of the skull, helping to explain part of the overall diversity of skull form in this remarkable clade.

TABLE OF CONTENTS

	Page
ACKNOWLEDGEMENTS.....	i
ABSTRACT.....	ii
TABLE OF CONTENTS.....	iii
LIST OF TABLES.....	v
LIST OF FIGURES.....	vi
GENERAL INTRODUCTION.....	1
CHAPTER 1: Evolution of Cranial Morphology: Analysis of Different Echolocating Groups.....	4
I. INTRODUCTION.....	4
II. MATERIAL AND METHODS.....	10
Geometric Morphometric Data Collection.....	10
Determination of Rostral Flexion.....	14
Quantifying macroevolutionary trends in rostral flexion.....	16
Is the evolution of rostral flexion associated with selection for echolocation type?.....	19
III. RESULTS.....	22
IV. DISSCUSION	32
Consequences of Rostral Flexion on Cranial Structure.....	32
Evolution of Rostral Flexion.....	35
Echolocation is linked to angle of rostral flexion.....	36

V.	CONCLUSIONS.....	39
CHAPTER 2: Functional Consequences of Extreme Rostral Flexion.....		40
I.	INTRODUCTION.....	40
	Functional Morphology of Biting.....	40
	Cranial Bite Force Resistance.....	42
	Bite Performance and Diet.....	43
II.	MATERIALS AND METHODS.....	46
	Calculation of Bite Force.....	46
	FE Analysis.....	47
III.	RESULTS.....	54
IV.	DISCUSSION.....	62
V.	CONCLUSIONS.....	66
REFERENCES.....		67
SUPPLEMENTARY MATERIALS.....		73

LIST OF TABLES

Tables	Page
1. Landmark placement data.....	13
2. Results of model fitting of rostral flexion evolution	31
3. Summary of muscle measurements.....	49
4. Summary of bite force results.....	57

LIST OF FIGURES

Figures	Page
1. Examples of shape diversity across all bat crania.....	2
2. Phylogeny of bat families.....	6
3. Placement of landmarks across all species.....	12
4. Highlight of landmarks representing rostral flexion.....	15
5. Sample figure of DTT analysis.....	18
6. Results of simmap reconstruction of echolocation mode.....	21
7. Distribution of rostral flexion across all families.....	24
8. Regression of landmark data on angle of rostral flexion.....	26
9. Results of DTT analysis.....	27
10. Phenogram illustrating the distribution of rostral flexion across bats.....	30
11. Natural and mathematically deformed (warped) <i>Mormoops</i> crania.....	50
12. Selected vs. Unselected areas showing rostrum vs. braincase/zygomatics....	53
13. Canine Unilateral Bite Stress.....	58
14. Canine Bilateral Bite Stress.....	59
15. Molar Unilateral Bite Stress.....	60
16. Molar Bilateral Bite Stress.....	61

GENERAL INTRODUCTION

The vertebrate cranium is a critical structure that supports discrete functional units; consequently, its overall form may represent a compromise reflecting biomechanical, developmental, and evolutionary factors associated with discrete functions. Bats (Chiroptera) have some of the most diverse crania among mammals (Rossoni et al., 2017). Across approximately 1,400 species throughout the world, bats exhibit many cranial shapes (Freeman, 1984). For example, species differ in cranial shape; some are elongated or flat faced, some possess nasal domes or tall sagittal crests, some have upturned or downturned snouts, and some have cleft palates or floating premaxillae (Fig. 1). Diversity in skull shape is not evenly distributed across bat lineages. For example, compared to other families, skull morphology is exceptionally diverse in the new world leaf nosed bats (Phyllostomidae). Because of large and unevenly distributed morphological diversity, bat skulls have become a major model system for understanding how traits evolve to adapt to different selective demands.

There are several physiological and ecological factors that impact diversification of skulls within bats, including sexual selection, habitat types, respiration, feeding, and in some, echolocation (Santana, 2016). Echolocation is a critical sensory modality that has experienced several significant evolutionary shifts in bats (and see intro to Chapter 1). Echolocation in bats appears to be an important evolutionary driver of skull morphology, and evolution associated with echolocation may have subsequently constrained morphological adaptations along other ecological axes, such as feeding (Arbour et al.,

2019 ; 2021). Many specialized diets have been described in bats, some of them unique among mammals (Freeman, 1984).

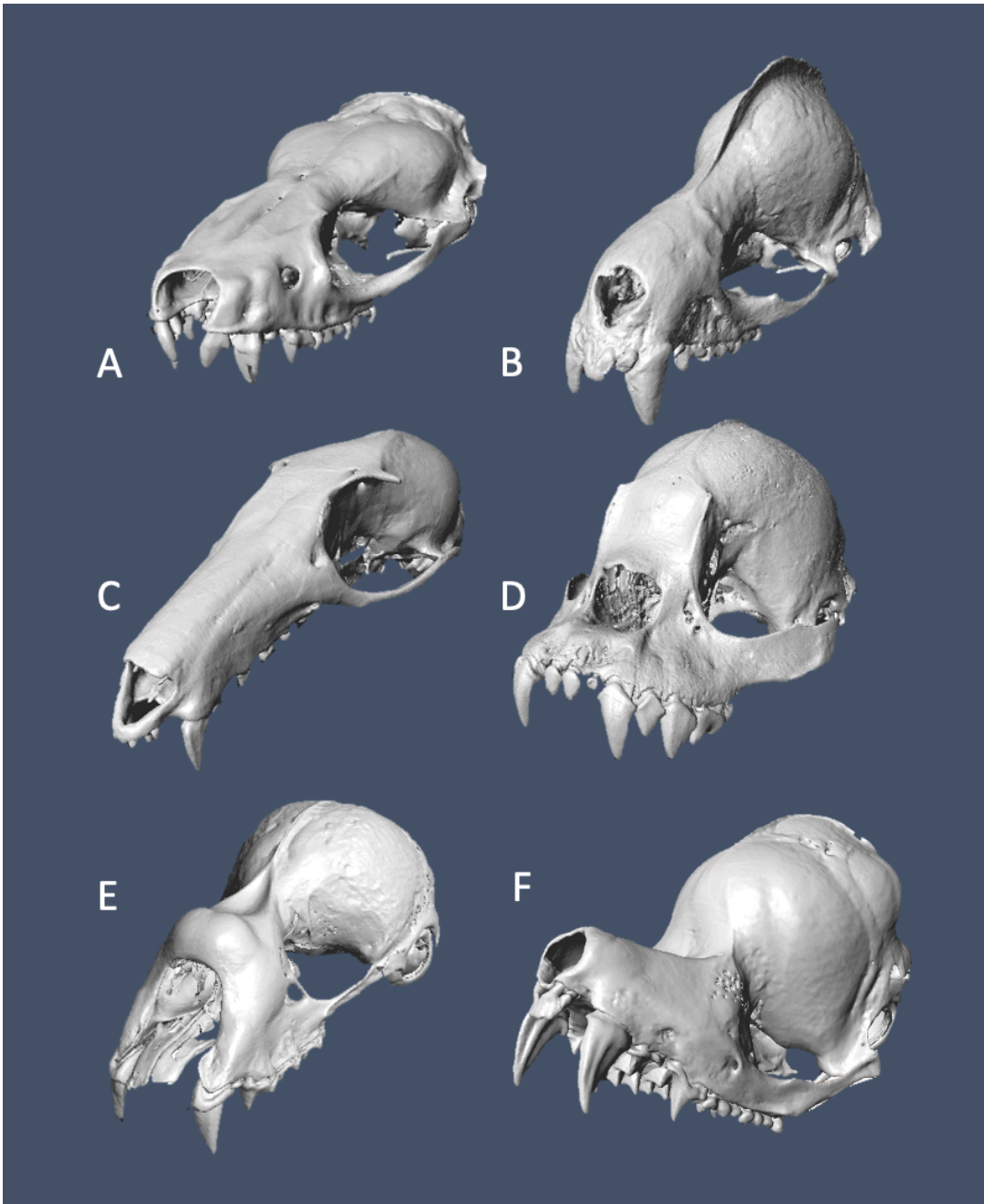


Figure 1. Examples of shape diversity across all bat crania. Flat vs. tall skulls (A vs. B), long vs. short rostra (C vs. D), downturn vs. upturn snout (E vs. F), and the cranium in the lower left side is an example of nasal domes and floating premaxilla (E). Top left also shows a cleft palate (A).

Below is the species and (family, echolocation type).

- A-*Sauromys petrophilus* (Molossidae, oral-echolocator)
- B-*Lophostoma silvicolum* (Phyllostomidae, nasal-echolocator)
- C-*Macroglossus sobrinus* (Pteropidae, non-echolocator)
- D-*Ametrida centurio* (Phyllostomidae, nasal-echolocator)
- E- *Rhinolophus simulator* (Rhinolophidae, nasal-echolocator)
- F- *Mormoops blainvillei* (Mormoopidae, oral-echolocator)

Although many species of bats are insectivores, others are carnivorous, piscivorous, frugivorous, nectivorous, and even sanguivorous (Freeman, 1984). Diversity of diet is great in one family in particular, the Phyllostomidae, which exhibit species specialized in most if not all dietary specializations known in bats. An association between skull shape and diet suggests that shape was under strong selective forces as novel dietary opportunities were discovered (Dumont et al., 2005). Although adaptations associated with feeding are well-studied in bats (Dumont et al., 2012; Santana & Dumont, 2009; Santana et al., 2012; Santana & Cheung, 2016), the evolutionary pressures on skull shape associated with echolocation have received less attention and, therefore, are not understood as well from a comparative context. Interestingly, high dietary diversity is found only in families bearing a particular echolocation mode (nasal-emission, and see intro to Chapter 1), suggesting that these two major functions (feeding and navigation) may experience selective trade-offs.

In this thesis, I examine the position of the rostrum (upturned vs. downturned) in bats, which is an aspect of skull shape in bats that has received little attention but has been linked to mode of echolocation (Arbour et al., 2019). In chapter 1, I describe the evolution of position of the rostrum and test for a direct selective connection to echolocation mode. In chapter 2, I quantify the potential biomechanical trade-offs associated with an extreme upturn of the rostrum.

CHAPTER 1: Evolution of Cranial Morphology: Analysis of Different Echolocating Groups

INTRODUCTION

Studying morphological diversity is important for understanding key evolutionary mechanisms as a response to different environments and selective pressures. Form and function are tightly (though incompletely) linked, and morphological variation within a clade can be indicative of adaptive processes that enable species to interact with their environment in different ways. Changes in morphology allow for the development of innovations or specialized functions to be possible, potentially allowing species to exploit new ecological opportunities and diversify into numerous lineages (Dumont et al., 2014). Conversely, shape change may also restrict a species diet, niche, or selective behaviors, thus limiting their abilities to exploit new opportunities. However, non-adaptive processes can also generate morphological diversity, and older clades are expected to be more diverse morphologically than younger ones simply as a result of random walk processes, such as genetic drift, in which variation arises without selective pressures (Arbour et al., 2019).

This high morphological diversity makes bat species an excellent model system for understanding the selective processes driving shape evolution. Previous evolutionary studies of bat skull diversification show three major patterns of variation: (1) length of crania (fig. 1, C = elongate vs. D = short), (2) shape of skull (fig. 1 A = flat vs. B = tall), and (3) shape of rostra (fig. 1, E = upturned vs. F = downturned) (Arbour et al., 2019). These cranial shapes were strongly partitioned in the early divergence of the clade and

shifts early in the evolutionary history of the clade appear to have evolved by echolocation type (Arbour et al., 2019). Later shifts in the cranial morphology, and most shifts in mandible shape, were driven by dietary preferences (Arbour et al., 2019). The bat skull, like those in most vertebrates, has several important functions, including feeding, supporting sensory structures, (olfactory sense, taste, hearing, vision, and communication) as well as some unique functions like echolocation. Morphological change due to dietary specialization among bats is a key factor influencing evolution of skull morphology. For example, many bats are insectivores, whereas others are carnivores, piscivores, frugivores, nectivores, or sanguivores (Freeman, 1984). However, dietary specializations are not evenly distributed across lineages of Chiroptera. Most families show limited dietary preferences (e.g., insectivores). Dietary specializations are more diverse in a few families (e.g., Phyllostomidae, New World leaf nosed bats). What causes this variability of diet in some clades but not others? Perhaps novel ecological diversification in the New World, or perhaps the morphological diversity of skull shape in this New World family results from constraints associated with multiple functions associated with the crania.

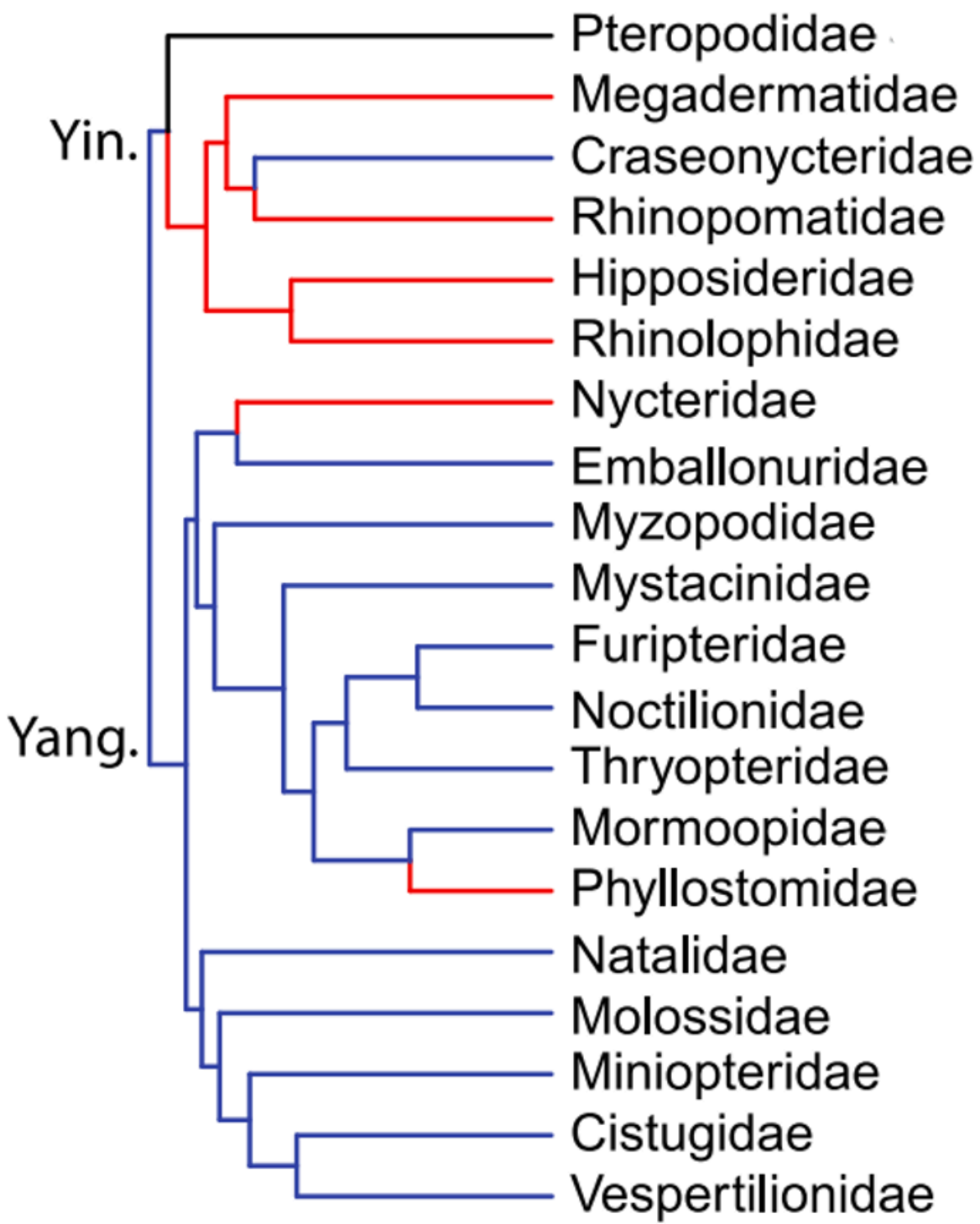


Figure 2. Phylogeny of bat families from Arbour et. al., (2021), reproduced with permission of the author. Yin. is an abbreviation of for Yinpterochiroptera and Yang. is an abbreviation of Yangochiroptera. Blue indicates oral-echolocators, Black shows non-echolocators, and red represents nasal-echolocators.

Echolocation is the capability of an animal to produce and emit the sound for the purposes of locating objects in their environment; after the sound hits an object it will bounce back to be received by the individual, providing information on distance and directionality of either structures or prey. Echolocation has evolved several times in distinct clades of Mammalia (e.g., chiropterans, cetaceans, shrews, and rats; Jones, 2009). In bats, significant shifts in the mode of echolocation evolved independently in distinct clades. In contrast to the more recent radiation of bat dietary specializations, adaptations in the method of echolocation appear to be ancient. Biologists recognize three general modes of echolocation in bats: oral-emitting, nasal-emitting, and non-echolocators. Nasal-emitters and oral-emitters both produce calls within the larynx but differ in the structure sound is directed through (nostrils or mouth). Most bats are laryngeal echolocators, except for the Pteropodidae (the "megabats") in the Yinpterochiroptera (Fig. 2, Yin.), and this family is the sister clade to several nasal-emitting families. Additionally, the sister clade to the Yinpterochiroptera - the Yangochiroptera (Fig. 2, Yang.) - is composed of laryngeal echolocating families, which suggests that earlier bats possessed laryngeal echolocation, and this trait was lost in the megabats (Thiagavel et al., 2018). Oral emission is likely the ancestral condition, and nasal emission likely evolved multiple times (independently within the Rhinolophidea, Nycteridea and Phyllostomidae) (Thiagavel et al., 2018). The relatively well-developed and larger eyes of pteropodids compared to other lineages of bats are presumably associated with a greater reliance on vision to locate food; consequently, these bats do not rely on the larynx to produce sounds associated with echolocation and have evolved unique echolocating mechanisms, such as tongue clicks and wing flaps (Jones & Teeling, 2006). These two types of

echolocation that do not involve the larynx are very rare, and the laryngeal production of Sound is not found in any member of this family; thus, they are referred to as “non echolocators” or “ non-emitters”.

Little variation in skull shape is due to feeding behavior; rather, echolocation type and foraging method may be of higher importance than the actual prey type itself (Freeman, 1984). More recent phylogenetic comparative analyses of cranial shape in bats have shown evidence of strong divergence of skull shape among the three major types of echolocators (Arbour et al., 2019). The relative rotation of the rostrum (compared to the rest of the skull) is a major axis of diversity and may be of adaptive significance to echolocation type. This was consistent with prior observations of bat skull shape variation suggesting that the upward deflection of the rostrum in oral emitters may permit calls to be directed more anteriorly during flight; whereas, the downturned rostrum of nasal emitters optimally positions the nostrils for echolocation calls (Pedersen, 1998). However, this prior study (Arbour et al. 2019) examined broad morphological trends using exploratory analysis approaches (e.g., PCA) and did not specifically examine the evolution of rostral flexion. Nor did this prior study examine the functional consequences of these major angles of the rostrum. Furthermore, an examination of the organization of shape variation in the bat skull further revealed a strong influence of echolocation type (Arbour et al., 2021). Oral-emitting bats showed much more modular skulls (i.e., different parts of the skull varied independently in their shape), but slower evolution than nasal-emitting bats which had more integrated skulls (different parts of the skull have more strongly covarying shape).

Although previous studies have examined the macroevolutionary trends of other major elements of bat skull shape (e.g., elongation), specific analyses into the evolution of rostral flexion are limited and predate the development of major phylogenetic comparative methods and statistical analyses of shape change (Arbour et al., 2019; Dumont et al., 2014; Santana et al., 2012). The objectives of this chapter are to (1) determine how much shape variation is linked to rostral flexion, (2) determine when and how this trait (rostral flexion) evolved within the history of the clade, and; (3) evaluate if echolocation type is an evolutionary driver of rostral flexion. To assess the variety of skull shape diversification among all three echolocator groups, I used a geometric morphometrics approach to demonstrate the complexity of shape and define an angle of rostral flexion (Kraatz & Sherratt, 2016). I assessed the shape evolution of the skull and rostral flexion using phylogenetic comparative methods and a previously published, phylogenetic tree based on extensive genetic sampling. I hope that a better understanding of how the diversity of rostral flexion in bats evolved and quantifying its potential connection to echolocation will help to explain why the diversity of skull morphology varies across bat clades and what macroevolutionary factors may have facilitated or limited the evolution of diverse crania.

MATERIALS AND METHODS

Geometric Morphometric Data Collection

I sampled crania from 235 species of bats, from 20 of the 21 recognized families, that included representatives of each echolocation type found in bats (118 oral-echolocators, 89 nasal-echolocators, and 28 non-echolocators). Landmark data on skull shape was obtained from STL files of 203 species from micro CT scans previously published (Arbour et al., 2019). Because oral-echolocators were proportionately underrepresented in these data, I included 32 oral-echolocating species obtained through 3D models (STL files) on the open-access repository Morphosource (<https://morphosource.org>). The shape of the skull was characterized by using landmark-based geometric morphometrics (Kraatz & Sherratt, 2016; Zelditch et al., 2004), which uses the cartesian coordinates (e.g., x, y and z) of homologous landmarks to characterize complex shapes. Using Checkpoint v. 2017, 26 landmarks were marked on homologous structures on the crania of all specimens (Table 1). I also digitized five curves using equidistant sliding semi-landmarks, which included the dorsal midline (semi-landmarks were placed starting from the anteriormost point on the midline of the nasals, then end at the intersection of the lamioindal and sagittal crests, blue dots in Fig. 3) and dorsal and ventral profiles of the zygomatic arches (the dorsal profile starting from the anteriormost inflection point of the orbit, ending dorsally at the upper posteriormost articulation of zygomatic arch with braincase (red dots in Fig. 3). The ventral profile started with the bottom anteriormost point of insertion of the zygomatic arch on the maxilla and ending at the lateralmost margin of the mandibular fossa (yellow dots in Fig. 3). All curves were oversampled and

resampled by length (29 midline semi-landmarks, 25 zygomatic semi-landmarks).

Missing landmarks (resulting from damage to skulls) were first imputed using reflected relabeling to exploit bilateral symmetry (a mirror image of the skull landmarks is Procrustes aligned with itself and missing landmarks are directly imputed), then using Bayesian PCA, as implemented in the functions “flipped” and “MissingGeoMorph” in the R package “LOST” (Arbour & Brown, 2014; Gunz et al., 2009).

All landmark coordinates were aligned using general Procrustes superimposition, which removes the impact of differing landmark rotation, position, and scaling by centering the landmarks, scaling all configurations to a centroid size of 1, and optimally rotating individual specimens to minimize the Procrustes sum of squares (Zelditch et al., 2004). Procrustes controls for all changes in orientation, scale, and position of the skulls, so only differences in shape are present. This technique provides a set of landmark coordinate configurations that are comparable among specimens. Landmark coordinates were then averaged by species and across the lateral midline by mirroring paired landmarks(Arbour et al. 2019).

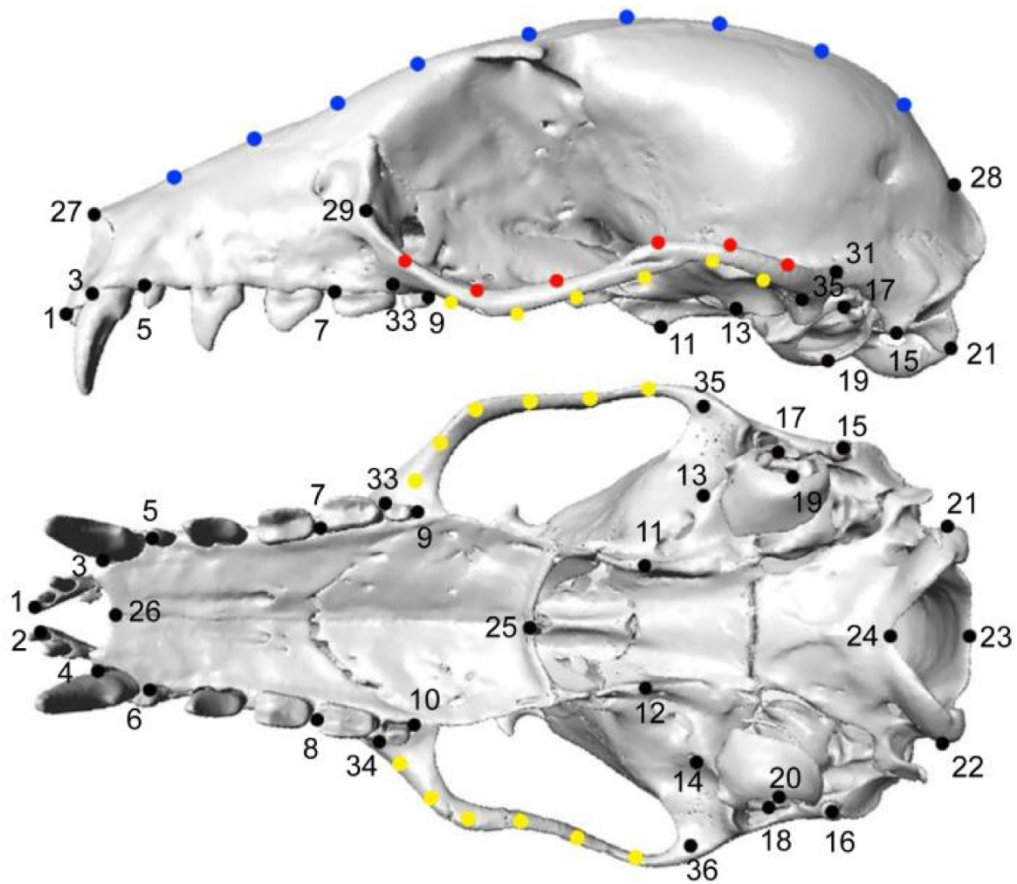


Figure 3. Placement of landmarks across all species as defined by Arbour et al., (2019) and used with permission from the author. Black dots represent landmarks (placement of landmarks shown in Table 1), and red, yellow, and black dots represent semi-landmarks. This image is taken from the supplementary material of Arbour et. al.,

Landmark	Location
1-2.	Anteriomost point of premaxilla
3-4.	Anteriomost point on canine alveolus
5-6.	Anteriomost point on premolar alveolus
7-8.	Anteriomost point on the first molar alveolus
9-10.	Posteriormost point on molars
11-12.	Ventralmost point on pterygoid hamulus
13-14.	Medialmost margin of the mandibular fossa
15-16.	Ventralmost point on mastoid process
17-18.	Dorsalmost point on the external edge of the auditory meatus
19-20.	Ventralmost point on the external edge of the auditory meatus
21-22.	Lateralmost point on occipital condyle
23	Dorsal border of foramen magnum
24	Ventral border of foramen magnum
25	Posteriormost point on midline of palate
26	Anteriomost point on midline of the complete palate

Table 1. Landmark placement data. This tables shows the landmarks used across all bat skulls. Landmarks were placed on the left side and then right side of the skull. The landmarks were used from Arbour et. al., 2019.

Determination of Rostral Flexion

To quantify the relative position of the rostrum as compared to the rest of the skull, I isolated four landmarks that described the anterior and posterior limits of the hard palate, and the midline of the foramen magnum (highlighted in Fig. 4) (Kraatz & Sherratt, 2016). Using custom code in R, I calculated the angle at the intersection of the lines formed by these four landmarks and use this angle as a measure of “rostral flexion” for all subsequent analyses. I applied this calculation to all 235 species and then converted from radians to degrees.

To determine the amount of overall variation in cranial shape linked to rostral flexion, I used a Procrustes regression as implemented in the R function “procD.lm” from package “geomorph” (Dean et al., 2022). This function carries out a general linear model type analysis but is modified to accommodate multi-dimensional landmark data (Collyer et al., 2015). I tested for a significant relationship between overall cranial landmark shape and rostral flexion and then determined the percentage of shape variation explained by rostral flexion by using the goodness of fit (R^2). Significance of the regression was assessed using randomized residual permutation as implemented in the R package “RRPP” (Collyer et al., 2015). Patterns of shape variation associated with high and low rostral flexion were visualized using the “geomorph” function “picknplot.shape”.

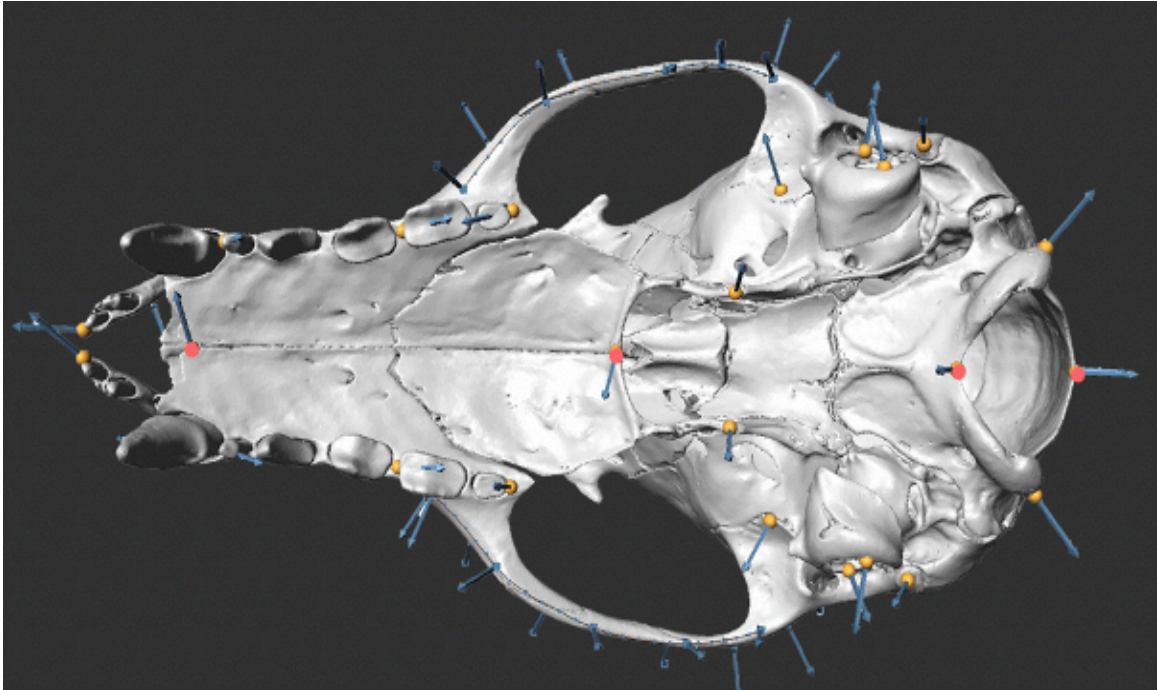


Figure 4. Highlight of landmarks representing rostral flexion. The yellow marks with arrows represent the landmarks. The blue dots (with arrows) represent the curves. The red dots display the four landmarks used to quantify rostral flexion. Landmarks were defined by Arbour et. al., 2019.

Quantifying macroevolutionary trends in rostral flexion

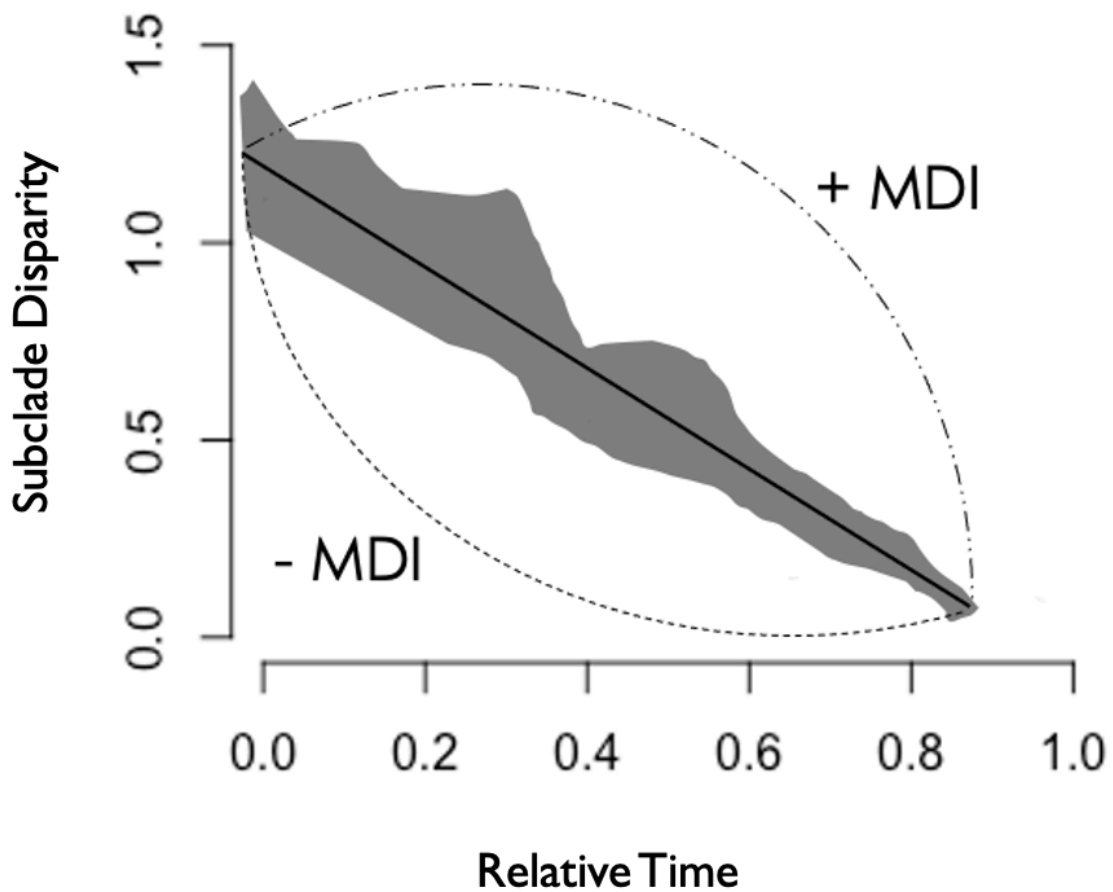
Trait disparity may accumulate under neutral (genetic drift) or active processes (selection, competition). I explored how the disparity of rostral evolution has accumulated through time across bats. Disparity through time analysis (DTT) describes how morphological traits have evolved within a given clade over time by calculating the average disparity of all subclades of a phylogeny present at a given point in time (Slater et al., 2010; Harmon et. al., 2003). The plot of the average subclade disparity vs. the age of the node is known as the observed DTT curve. I compared this curve to expectations under a neutral, constant rate process. Brownian Motion (BM) is a constant rate, random walk model, governed by a rate parameter (σ^2) used to represent evolutionary processes like genetic drift. I simulated 100 sets of character evolutions for rostral flexion under a BM evolutionary process, based on the best fit rate parameter and the phylogeny of all included species. The average subclade through time of all simulated character histories was used as an expectation for a DTT curve under a neutral process.

Divergence from a random walk, constant rate process in DTT is quantified using the morphological disparity index (MDI), which is the area between the observed and average simulated BM curve. Negative MDI values are often indicative of early rapid rates of trait evolution, with later slowing and stabilization of evolution (Arbour et al., 2019; Slater et al., 2010). This early establishment of trait diversity leads to a pattern of strong divergence in basal lineages. Positive MDI values may be indicative of either increasing rates of evolution through time, or strong selection towards a single selective peak (Arbour et al., 2021; Feilich & López-Fernández, 2019). MDI's close to zero

indicate a mostly constant rate, BM process. An example of a DTT plot is shown in Fig. 5.

I predict that rostral flexion was an important factor in the early evolution of skull shape in bats, due to a potential link with echolocation mode (and see *Is the evolution of rostral flexion associated with selection for echolocation type?*). I assessed whether the observed MDI value was likely to have been produced under a constant rate BM process, by calculating the MDI of each individual simulated DTT curve as compared to the average BM simulation. The p-value for the test was the proportion of simulated curves that produced a lower MDI than observed MDI value. Calculation of DTT curves, MDI and significance of the MDI value was accomplished using the function “`dt`” in the R package “`geiger`”. I also use the “`dt`” function to generate a DTT plot comparing observed DTT with the null, Brownian Motion (BM), (Colombo et al., 2015). A negative MDI is associated with the trait evolving early in the clade’s history, in accordance with an early burst evolutionary model.

Figure 5. Sample figure of DTT analysis. Dotted dashed line represents a positive MDI, meaning that the individuals are accelerating rates of evolution or experiencing selection. The dashed line is representing a negative MDI. This shows that the organism diversified early in the clade history, supporting an early burst model.



Is the evolution of rostral flexion associated with selection for echolocation type?

I visualized the overall pattern of macroevolution of rostral flexion in the context of echolocation mode across all bats using function “phenogram” in the R package phytools, and a subtree of the Shi and Rabosky (2015) all bat phylogeny. The function phenogram rearranges a previously established phylogeny to fit a continuous phenotype (the y axis) through time (x-axis). I reconstructed the evolutionary history of echolocation mode using “simmap” (Bollback, 2006). Simmap uses stochastic character mapping to reconstructed evolution of discrete characters and map them onto a phylogeny. Echolocation mode was described as one of three states for each species (non-echolocator, nasal echolocator and oral-echolocator). The assessments for each species follow Arbour et al., (2019), except the additional species included from Morphosource, which were all oral emitters. I used an asymmetric transition rate matrix (model = “ARD”) and assigned a prior state of oral echolocation to the root node, based on fossil and comparative evidence that indicates this is the ancestral echolocation mode of bats (Thiagavel et al., 2018). I mapped echolocation mode onto the branches in the phenogram.

I used maximum likelihood model fitting to test whether the evolution of rostral flexion is associated with echolocation mode across bats. I tested whether echolocation mode drove either a (1) change in selection on rostral flexion, (2) a change in the evolutionary rate, or (3) both. I used both BM and Ornstein-Uhlenbeck models in our model fitting analyses. Ornstein-Uhlenbeck (OU) models extend BM models to incorporate selection towards a particular trait value by including a parameter for the strength of selection (α) and one or more values for selective optima (θ), as well as one or

more rates of evolution (σ^2). Using a maximum likelihood approach, I compared BM and OU models that differed in (1) the number of evolutionary rates (V), and (2) the number of selective peaks (M), based on echolocation mode (Beaulieu et al., 2012). I also included models representing simple, single rate BM evolution (BM1), and single peak OU evolution (OU1). I compared the fit of all models using Akaike Information Criterion (AIC), where the lowest AIC represents the best fit model. The ΔAIC of each model was calculated as the AIC of a given model – the best fit model (best fit model $\Delta AIC = 0$). Following Burnham and Anderson (2002), I used a cutoff of $\Delta AIC = 2$ to indicate the best fit model which showed improved support to all other models. All maximum likelihood model fitting was implemented using the R package “OUwie” (Beaulieu et al., 2012). Models were fit for each of the 100 simmap reconstructions of echolocation mode evolution, and the results are summarized in Table 2.

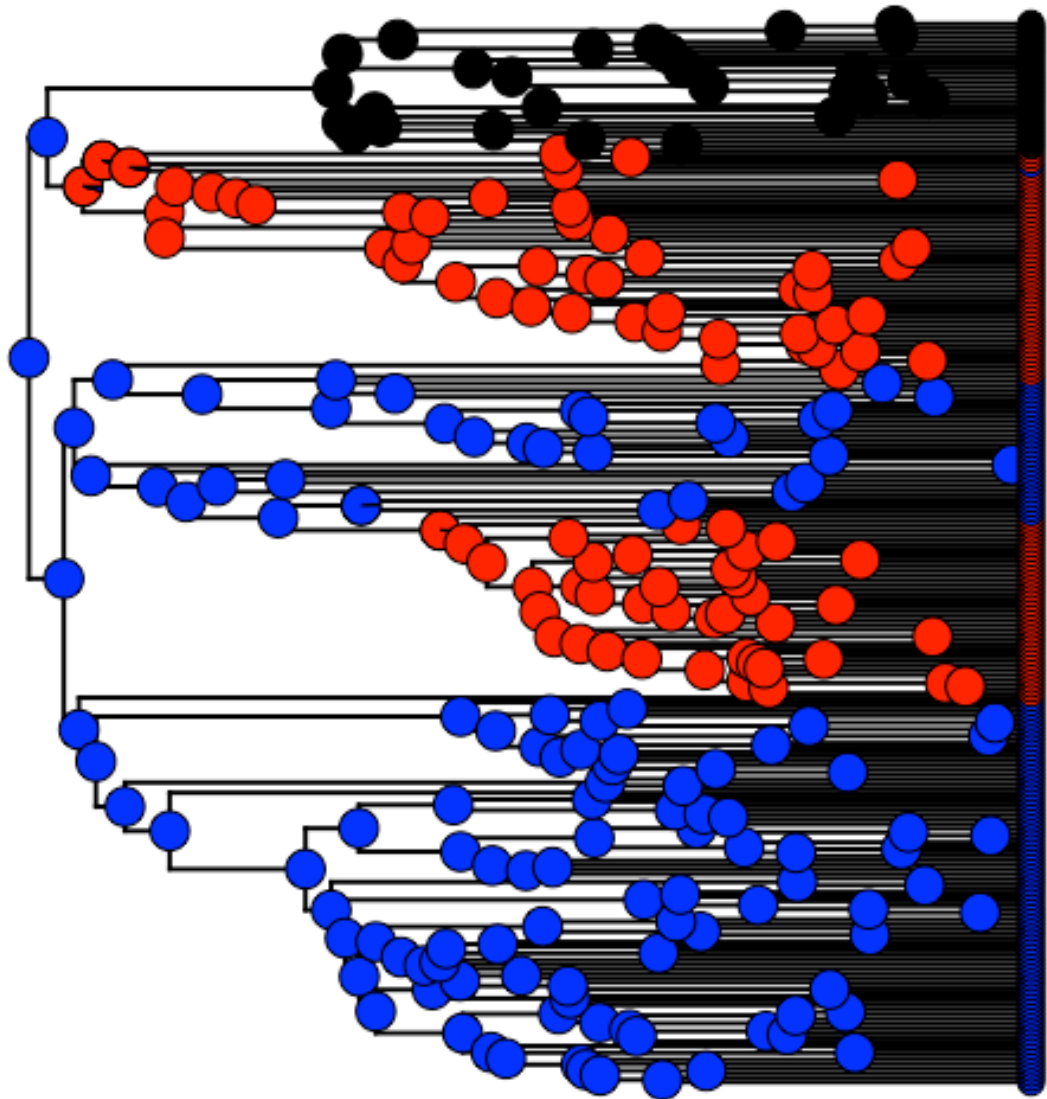


Figure 6. Results of simmap reconstruction of echolocation mode (circles). Blue = oral emitters, Red = nasal emitters, Black = non-echolocators.

RESULTS

The angle of the rostrum (rostral flexion) was calculated for all 235 species (Fig. 7). The rostral flexion ranged from lowest angle of 75.07° (*Mormoops megalophylla*; Mormoopidae) to the highest angle, 186.66° (*Rhinolophus philippinensis*; Rhinolophidae). The mean angle of the rostrum was 138.32° . The pteropodids (Flying Foxes) tend to have more average rostral angles (118.12° – 157.59°). Phyllostomidae on average showed 20° higher flexion than average across all bats (131.87° – 163.13°). Vespertilionidae tend to have lower than average angles associated with the rostrum (90.58° – 141.75°) (Fig. 7).

Pteropodidae (non-echolocators) tend to have a trend toward a more average rostral flexion (mean = 140.85°). Within the Yinpterochiroptera, there are several nasal-echolocators and one family that has experienced a reversal to oral echolocation; in this monotypic family (Craesonycteridae) I had one representative specimen, and the rostral angle of this individual was 137.89° . The closest relative of Craesonycteridae, is a nasal-echolocating family, Rhinopomatidae, whose mean (145.29°) was above average and about 8° higher than Craesonycteridae, thus showing a clear divergence in rostral angle. Also, within the Yinpterochiroptera, the Rhinolophidae family shows the highest mean flexion (169.12°) (all species rostral flexion angles are included in SUPPLEMENTARY MATERIALS).

Although composed predominantly of oral-echolocating families, nasal echolocation evolved twice within the Yangochiroptera (Fig. 2). Nycteridae had a mean rostral flexion of 170.23° , which is substantially larger than the presumed sister family,

the Emballonuridae (135.48°), which comprises oral echolocating species.

Phyllostomidae represent an above average mean at 148.37° and Mormoopidae is the lowest mean angle at 97.30° . Finally, Vespertilionidae is below average at 118.86° (Fig. 7).

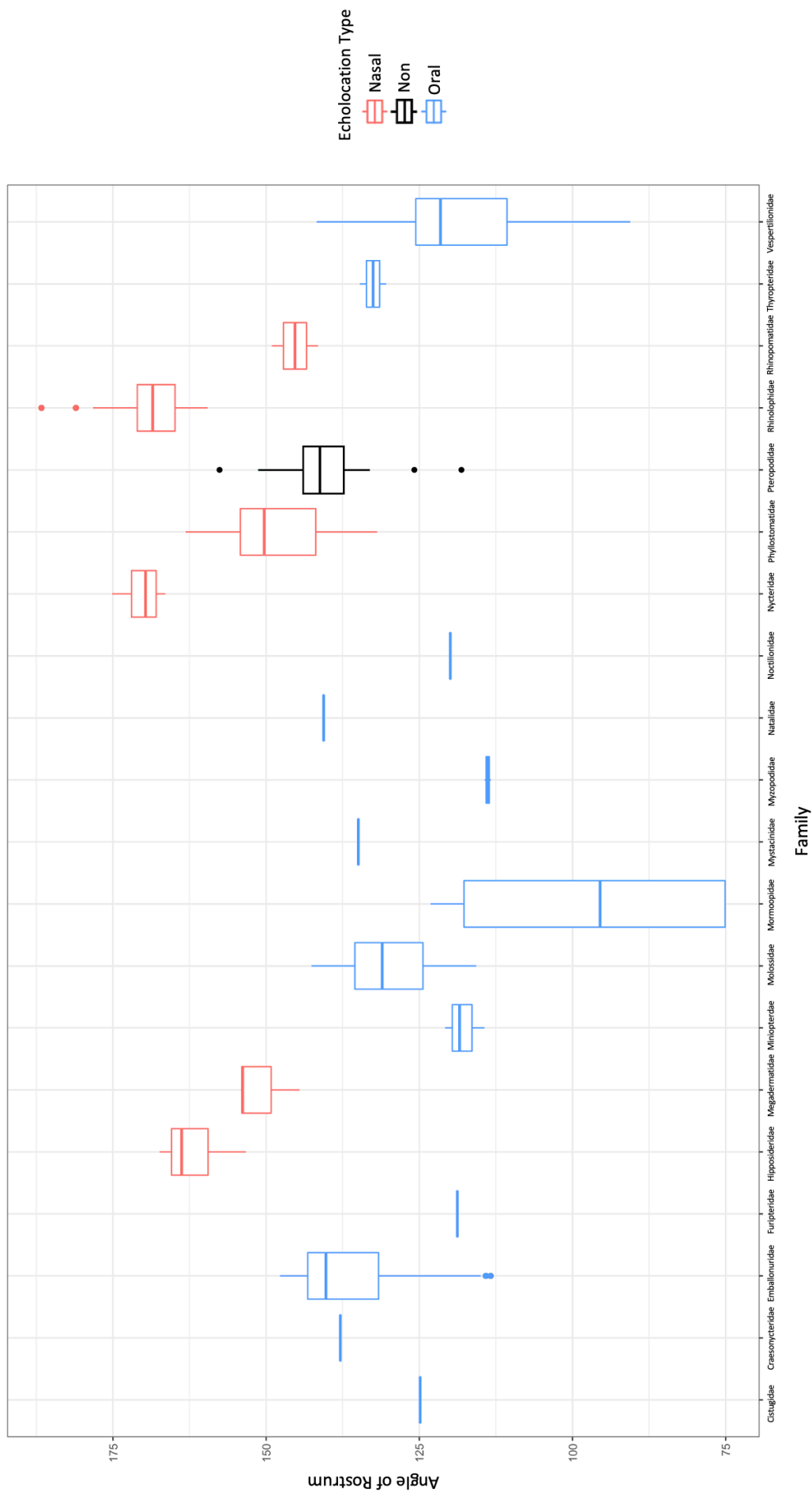


Figure 7. Distribution of angle across all families

Rostral flexion is of importance to overall cranial shape variation given that the Procrustes regression of shape variation was significant ($F = 113.17$, $p = 0.001$) indicating that rostral flexion contributes to overall cranial shape variation. Rostral flexion explained approximately a third (32.7%) of overall cranial shape variation across all species of bats. Interestingly, other features of shape variation throughout the skull (independent of the rostrum) were associated with rostral flexion. For example, lower values of flexion of the rostrum (i.e., upturned) drives shape change in the zygomatics by causing a lateral expansion, lengthening, and shifting upward of the hard palate, and shifting the pterygoid hamulus posteriorly (Fig. 8). In species with higher rostral flexion, we observed zygomatic compression (, medially), shortening of the palate, and the anterior shift the pterygoid hamulus. Cranial shape changes and rostral flexion were similar in nasal and oral emitters (Fig. 8, blue and red points), but those of non-echolocators were different (Fig. 8, black).

Disparity through time analysis showed that disparity in rostral flexion was partitioned early in the evolution of bats (Fig. 9). The observed MDI value of -0.2358 was unlikely to have occurred under a constant rate process ($p < 0.001$). The observed trait DTT curve (solid line) also did not fall in the gray area representing all 100 simulations of Brownian Motion and is therefore unlikely to have occurred under a constant rate evolutionary process. Rostral flexion largely evolved quickly in early bat lineages and varied less substantially towards the present.

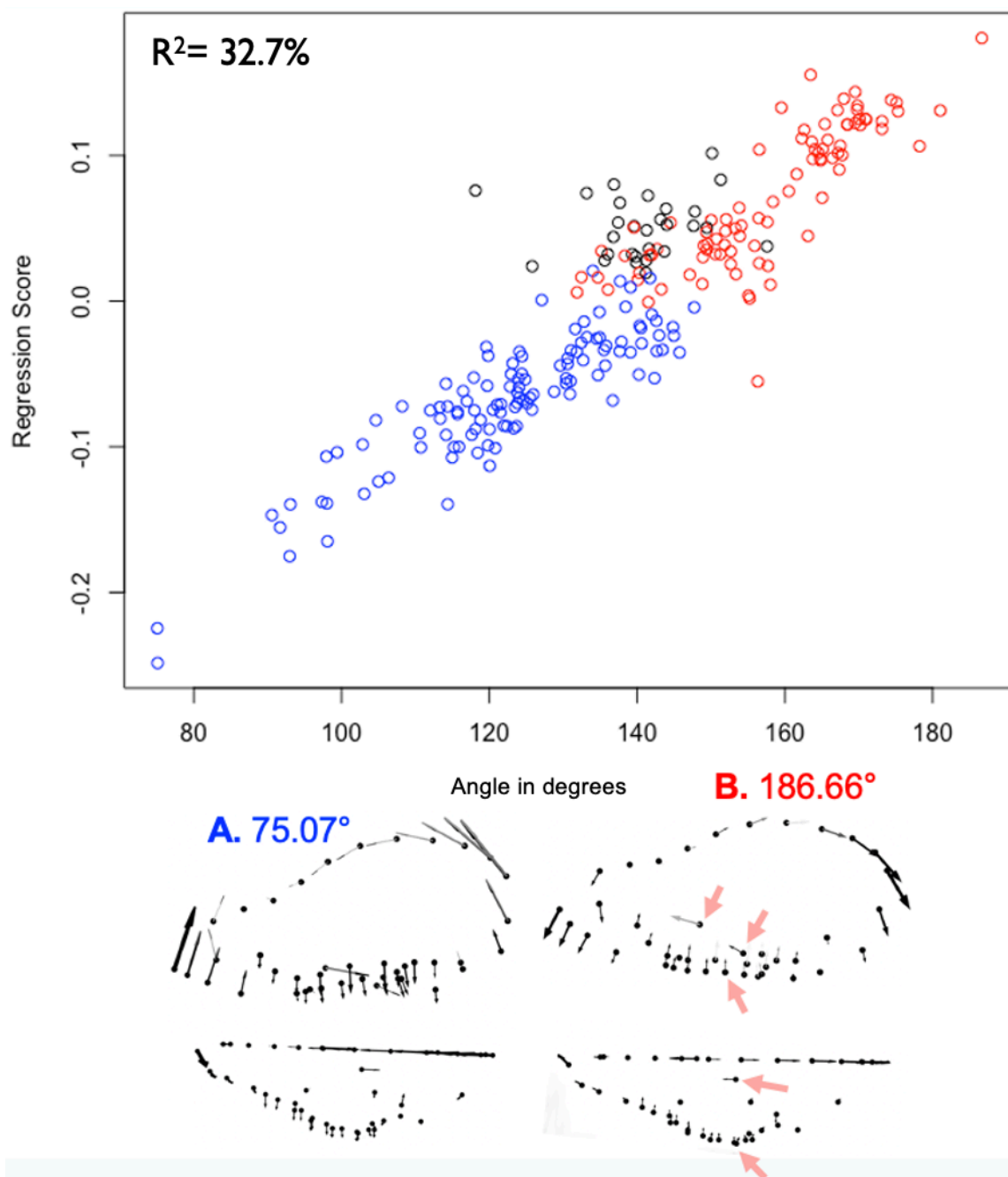


Figure 8. Regression of landmark data on angle of rostral flexion (x-axis). **A** is a representative of the oral-echolocating group, with the lowest angle of rostral flexion. The dots show the average skull shape landmarks in all 235 species and the black arrows show the movement of those landmarks associated with the angle shown. The same is shown with **B** but with the highest angle of flexion. The red arrows are highlighting other parts of the skull that shift, along with flexion (e.g., zygomatics, pterygoid hamulus, basicranium).

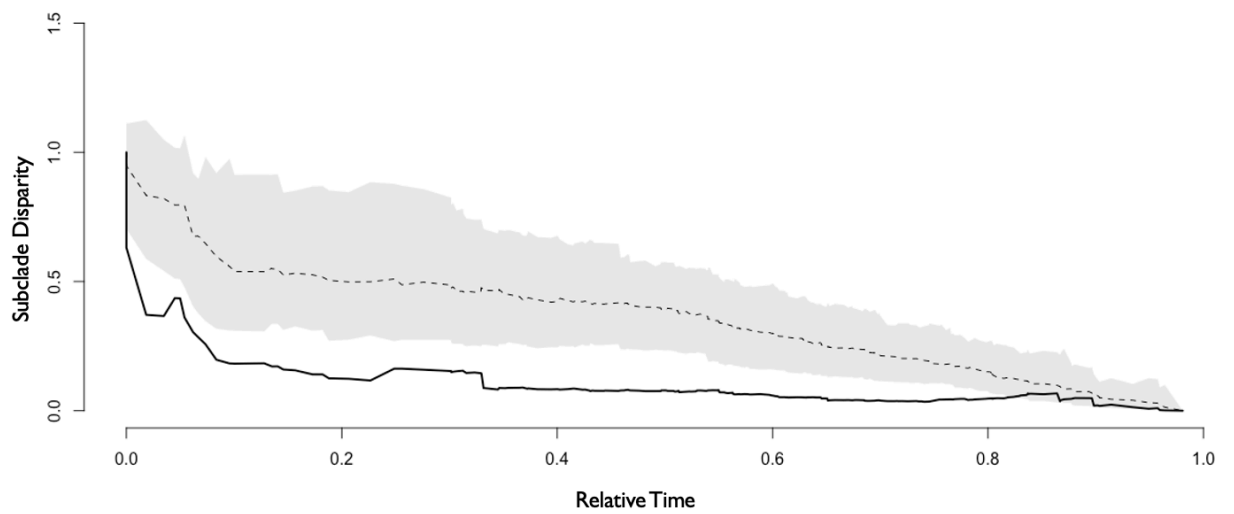


Figure 9. Results of DTT analysis. The grey area is 100 simulations of Brownian Motion. The dotted line represents the average Brownian Motion. The black line is rostral flexion.

Nasal echolocators appeared to have evolved toward a higher degree of rostral flexion based on the phenogram of rostral flexion (Fig. 10); whereas, non-echolocators seemed to have evolved toward the mean degree of rostral flexion (138.32°). Oral echolocators appear to have evolved towards much lower than the mean rostral flexion (lower angle). Each of the three transitions (Rhinolophidea, Nycteridae and Phyllostomidae) from oral to nasal echolocation (highlighted with arrows, Fig. 10) appeared to be associated with a transition from a lower degree of rostral flexion to a higher degree associated with nasal echolocation. Overlap in rostral flexion was most evident between the nasal emitters and non-emitters, especially among the phyllostomids and pteropodids (Fig. 10). Non-echolocators overlapped entirely with rostral flexion values observed in species with all echolocator types, but both oral-emitters and nasal-emitters showed ranges that included unique values not found in the other two groups (Fig.10).

Based on maximum likelihood model fitting, the best fit model was an OU model with both multiple peaks and multiple rates associated with echolocation mode. This model was strongly favored over all other models (minimum $\Delta AIC = -247.5985$), $\Delta AIC = 0.0$ ($K=7$) (Table 2). Oral emitters evolved toward a rostral flexion of about 124° ($\theta=123.68$), which fell in the middle of the range of observed values in these species. Nasal and non-echolocators are experiencing selection toward a more downturned rostrum, with values of the selective peaks falling outside of the currently observed range of the clade (Table 2), respectively. Optimum values outside of the observed range is a possible outcome of model fitting if clades evolve slowly or experience relatively weak selection towards a distant peak, or are experiencing more directional selection (Collar et

al., 2009). In addition to difference in optimum values, echolocation type was associated with a difference in evolutionary rate. Nasal echolocators had the lowest rate of evolution (Table 2, σ^2) . Oral and non-echolocators have both evolved nearly twice as fast as nasal echolocators (Table 2).

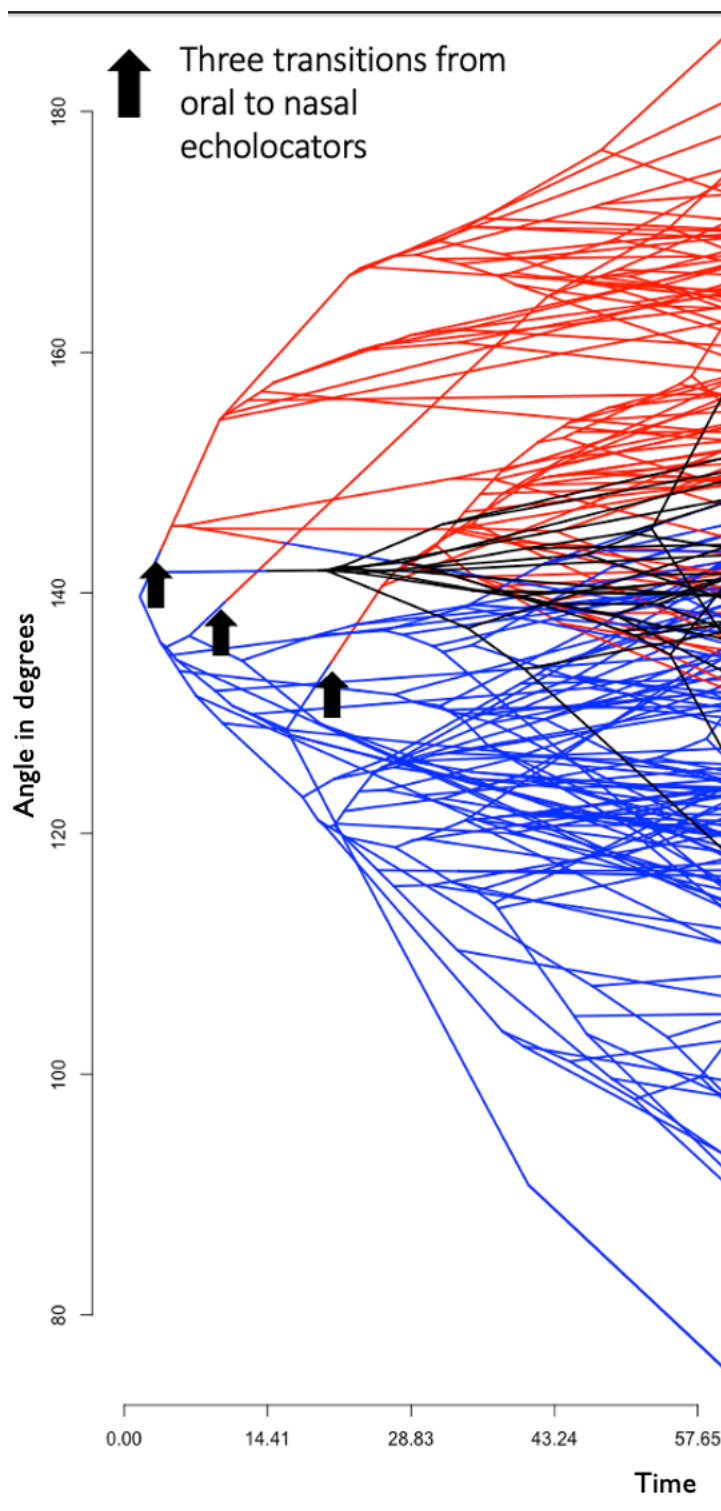


Figure 10. Phenogram illustrating the distribution of rostral flexion across. Blue representing oral echolocators, red- nasal echolocators and black – non echolocators.

Table 2: Results of model fitting of rostral flexion evolution. M= multiple peaks,

V= multiple rates associated with echolocation mode (nasal/non/oral).

Model Name	K	ΔAIC	Rates (σ^2)
BM-1	2	53.2	0.052
OU-1	3	44.8	0.052
BM-V	4	55.3	0.028 / 0.057 / 0.072
OU-M	5	10.7	0.043
OU-MV	7	0.0	0.025 / 0.056 / 0.052

DISCUSSION

Consequences of Rostral Flexion on Cranial Structure

Bats exhibit a remarkable diversity of cranial morphologies, and comparative analysis indicates that rostral flexion is a major component of this variation (Arbour et al., 2019, this study), explaining nearly one third of all cranial shape variation (this study). Furthermore, our data supports that suggestion that flexion of the rostrum is of adaptive significance to echolocating types, with evidence of macroevolutionary selection on this feature associated with shifts between echolocation modes, non-echo-locators have median flexion, nasal-locators have greater flexion, and oral locators have lower than average flexion (Table 2). Rostral flexion represents a major reorientation of the rostrum and basicranium relative to one another, but other features of the skull also change in association with rostral rotation. In oral echolocators (lower angle of rostral flexion), the zygomatic arches are displaced laterally. The lateral displacement away from the skull results in the zygomatic arches having a greater surface area, potentially resulting in a larger area for attachment of the masseter and zygomaticomandibularis muscles, and greater space to accommodate larger volumes of masseter and temporalis muscles. Each of these muscles contribute force required for biting and chewing. The change in upward shift of the basicranium may also change the angle of insertion of the temporalis muscle, which impacts the transmission of force from jaw closing muscles. The reorientation of the skull may actually bring the temporalis muscle closer to a 90-degree angle of insertion, where force transmission is optimized. The repositioning of the temporalis muscle relative to the jaw may have improved force transmission (i.e., a lower

bite force) because the length of the muscle fibers decrease. However, the shortening of the basicranium potentially limits the surface area for attachment of the temporalis muscle. If so, force production could be reduced. The origins of the masseter, another major jaw closing muscle, likely is affected less because its insertion on the mandible shifts as the upper jaw becomes repositioned. Finally, the pterygoid hamulus shifts posteriorly, which also affects surface area available for muscle attachment (the lateral and medial pterygoids are associated with biting and jaw opening respectively). The shift of the hamulus results in shorter muscle fibers, potentially increasing physiological cross section area (or PCSA), however the overall size of these muscle may decrease as well and overall impact of the change in cranial structure is difficult to predict. The change in muscle attachment points may reflect a constraint associated with upward tilt of the rostrum. With a decreased area of muscle attachments, this would restrict bite force which may be related to the idea that most oral echolocators are restricted in diet to be predominantly insectivorous (i.e., Vespertilionidae) (Herrel et al., 2008).

For nasal echolocators with a higher angle of the rostrum, the zygomatics are compressed medially thus reducing surface area for masseter attachment and less space to accommodate the major jaw closing muscles. The basicranium is shifted downward potentially increasing the surface area for muscle attachment of the temporalis, but the angle of insertion on the coronoid process may also be impacted as compared to oral echolocators, potentially decreasing muscle force transmission. The pterygoid hamulus shifts anteriorly, potentially increasing length of muscle fibers and decreasing the force they can exert; alternatively, the shift in the pterygoid hamulus could lead to an increase in the overall size of the muscles (and increase force generated. An increase in

attachment area and fiber length of the temporalis muscle and a decrease attachment area on the zygomatic arch for the masseter muscle may facilitate wider gapes, which is necessary for many nasal emitters bats with dietary specializations (i.e., phyllostomids) (Santana, 2016). Overall, the specific biomechanical consequences of rostral rotation on bite force cannot be assessed without further collection of myological data (e.g., fiber lengths, muscle masses, angles of pennation and insertion), but the overall changes in skull shape suggest that selection on different muscle attributes (e.g., size, fiber length, angle of insertion, areas of attachment) likely differ between oral and nasal emitters.

The upward tilt in the hard palate of oral emitters potentially enhances the efficiency of echolocation by allowing bats to emit the sound directly in front of them during flight and while foraging (Pedersen, 1998). The downward tilt in the hard palate of nasal emitters creates a tilted rostrum that aligns the nasal cavity directly in front of the bat as it seeks prey (Jones & Teeling, 2006; Pedersen, 1998). The shortened palates of nasal emitters (with downturned rostra) may be associated with nasal domes in some species. For example, many rhinolophoid species with nasal domes also have elongated turbinals that extend well past the hard palate (Curtis & Simmons, 2017). These structures potentially impact call production, while limiting impacts on sound production, and a shortened palate may contribute to their function. However, not all nasal-emitters possess elongated turbinals, and their function is not entirely understood.

The rostrum in oral emitters was also previously found to be shorter than the rostrum of nasal emitters, presumably for efficient echolocation (Pedersen, 1998). Interestingly, bats able to withstand strong torsional load (e.g., twisting forces) from unilateral (one-sided) biting of hard foods tend to have shorter skulls and greater reliance

on the temporalis muscle rather than the masseter muscle during jaw closing, at least in nasal-emitting taxa with relatively downturned rostra (Santana et al., 2012). This analysis may not accurately reflect echolocation by the exclusion of species with larger and more widely spaced zygomatic arches associated with upturned rostra. Therefore, studying feeding biomechanics chiefly in nasal emitting phyllostomid bats, which are often used as a “model system” in ecomorphological studies, may bias the importance of particular muscles/structural adaptations. Oral emitting families tend to have less elongate skull more suited to torsional loading than non-echolocators or nasal emitters (Arbour et. al., 2019).

Evolution of Rostral Flexion

DTT analysis shows that rostral flexion strongly structured overall cranial shape diversity across bats, and that these major aspects of skull shape evolved very early in bat skull evolution (as evidenced by the negative MDI). The evolution of this trait early during the diversification of bats may have greatly affected skull shape in various lineages. Further ability to evolve differently shaped crania can be constrained by changes in such foundational traits that drastically reshape the morphology of the skull. For example, in dinosaurs, major modifications of the skull associated with the evolution of avian lineages lead to decreases in the rate of evolution across several cranial features, especially those associated with feeding biomechanics (Larouche et al., 2020). Oral emitting taxa show a much more limited range of cranial elongation compared to nasal-emitting bats, as well as somewhat lower variation in the dorsoventral compression of the

skull (Arbour et al 2019). However, both oral- and nasal-emitting taxa show greater skull shape variation than non-echolocation pteropodid bats.

Perhaps the relative similarity of skull shape in several nasal and non-echolocating groups occurs because of the early split of bats into non or nasal echolocators, as seen in the Fig. 10 - although there is overlap in flexion with all three echolocating types. The similarity between nasal-emitters and non-echolocators may represent an evolutionary relict (non-echolocators evolved from nasal emitters rather than oral emitters) or may be associated with a functional trade-off. The return to a focus on sight for navigation may similarly impose constraints on upward rotation of the rostrum. However, the earliest bats were likely oral echolocators that possessed a more upturned rostrum, which may have allowed for more diversification in rostral flexion in early lineages. The rotation of the rostrum may be more critical for some types of echolocation - it may be more important for nasal echolocators to possess a downturned rostrum for feeding, along with other characteristics seen in skulls of nasal emitters (i.e., nasal domes). Comparatively, the higher diversity of rostral flexion values suggests that oral-emitters are more flexible, and that an average flexion (138.32°) is sufficient, though perhaps not ideal, to accommodate oral-emission of calls.

Echolocation type is linked to angle of rostral flexion

Model fitting analyses shows that rostral flexion experiences selection towards different adaptive optima depending on echolocator type, consistent with patterns observed in earlier studies (Arbour et al., 2019). Additionally, model fitting shows that rostral flexion in nasal emitters evolves slower than the observed rate in non and oral

emitters. Nasal emission has evolved multiple times from oral emission but has never reverted. The change in evolutionary rates may contribute to this pattern – the evolution of nasal emission may impose strong selection and a “dead-end” in terms of variation in this trait, preventing the evolution of traits necessary to reacquire oral-emission.

However, although nasal emitters evolve slowly in terms of rostral flexion, other work has shown that nasal emitters evolve other aspects of skull shape more rapidly than non-nasal emitting bats, including both aspects of cranial shape as well as faster evolution of the mandible (Arbour et al., 2021). Comparatively, mandibular shape in oral emitters evolves quite slowly, in contrast to both nasal-emitters and non-echolocators, thus greater diversification in this single trait (rostral flexion) does not enable morphological diversification of other traits. Rather, nasal emitters show a greater variety of structural innovations - bulbous bony nasal domes, largely detached and floating premaxillae, and elaborate fleshy nose leafs (disk shaped structures around the nasal opening) occur across nasal-emitting families, likely to make nasal emission more efficient (Arbour et al., 2021). The slower evolution of the rostral flexion in nasal emitters presents an interesting question. Are there constraints associated with rostral flexion in nasal emitters?

Interestingly, slow evolution of rostral flexion is in contrast with the high diversity of dietary specializations; nasal-emitting families like Phyllostomidae possess most if not all diets observed across all bats (insectivores, carnivores, piscivores, omnivores, frugivores – both soft and durophagus, nectivores, and sanguivores). In contrast, oral echolocators, which possess a faster rate of evolution, feed predominantly on insects. More diverse diets may have a tradeoff with evolution of rostral flexion. Previous studies that indicate the adaptive radiation of phyllostomid bats was driven by

the ecological opportunity present in the New World (Arbour et al., 2019; Rossoni et al., 2017). Enhanced cranial shape diversification was likely only possible in this clade as a result of the combination of more downturned rostra and the availability of dietary niches to diversify into. This would help to explain why other nasal-emitting clades do not show the same diversity of skull shapes as Phyllostomids. Perhaps there are more constraints associated with other shape changes associated with rostral flexion (i.e., zygomatics, pterygoid hamulus, etc.). These other shape changes may allow for dental and muscle adaptations within nasal echolocators providing for diverse diets as well, but only in the presence of available ecological niches as experienced by Phyllostomids. Interestingly, there are many traits associated with cranial elongation in nasal echolocators (Arbour et al., 2019). Although the evolution of rostral flexion slowed in nasal emitters, it spurred subsequent evolution on other trait axes in groups presented with unique ecological opportunities.

Furthermore, nasal emitters may experience slower rostral flexion because of integration of the cranium rather than a modular cranium (Klingenberg, 2014). Modularity is the separation of certain traits into modules that have a stronger correlation within a module than with features in other modules (Arbour et al., 2021). In essence, modular traits vary separately while integrated traits vary together (Arbour et al., 2021). Oral echolocators are more modular, which may help to explain the higher evolution rate - the front and back of the skull are able to evolve more freely from each other.

CONCLUSIONS

Rostral flexion contributes to one third of cranial shape variation found in bats, and the type of echolocation plays a major role in this variation by affecting the angle of rostral flexion. Several major attachment sites of muscles are also impacted by selection towards different shapes associated with an upturned or downturned rostrum, and therefore there are significant biomechanical implications for this major restructuring of overall form of the bat skull. Early evolution of the defining characteristic may have decreased the rates of evolution of rostral flexion, particularly in the nasal-emitting groups, with significant implications for the bats subsequent ability to evolve their cranial shape and to transition to other echolocation types. However, the biomechanical consequences associated with the development of extreme rostral flexion has not been studied and understanding the functional implications of this trait would help to further clarify the macroevolutionary patterns observed in this chapter

CHAPTER 2: Functional Consequences of Extreme Rostral Flexion in *Mormoops*

INTRODUCTION

The relationship between form and function in organisms is complex and poses many evolutionary conundrums, such as tradeoffs to morphological diversity and fitness. For example, the lower jaw of vertebrates acts as a lever system. The relative lengths of the components of the jaw (form) will result in changes to the mechanical properties of the lever (function). Furthermore, most simple levers experience a trade-off between force and velocity transmission – longer jaws are often “faster” than shorter jaws, which are “slower” but “stronger”. The functional consequences of changes in morphology (form) may be predictable for some anatomical systems, such as the jaw lever. However, for more complicated structures, such as the vertebrate cranium, the consequences of changes in form on the resulting function may be harder to predict. For example, individuals with a shortened skull are able to consume tougher foods compared to those with lengthened skulls, but the shortened skulls are relatively inefficient for capturing fast or large prey. These relationships are not linear and may include many inputs that affect function, such as bone, muscles, gape size, and body size.

Functional Morphology of Biting

Bite force has a clear function in the life of an organism and can contribute to many life history traits associated with defense, mating, competition, and feeding (Maestri et al., 2016). Bite force (function) is determined by several anatomical properties of the vertebrate skull (form). The jaw is considered a third-class lever (Kerr,

2010). In this lever system, the jaw adductor muscles (temporalis and masseter) would act as the input force (or effort), the fulcrum being the temporomandibular joint (TMJ), the output (or load) is the bite force (Kerr, 2010). In such levers, the mechanical advantage is the ratio between the in-lever length (the fulcrum to the coronoid process) and the out-lever length (the fulcrum to the teeth) and determines the mechanical properties of the lever. Having a low mechanical advantage (the relative lengths of the in-lever and out-lever of the jaw) would be beneficial for species with a softer diet but requiring quick movements (Santana et al., 2012). Having a high mechanical advantage is beneficial to species with a harder diet (Santana et al., 2012). With this being said, there are several other factors that may have an effect on bite force in bats. Another factor that affects bite force is the physiological cross-sectional area or PCSA. PCSA is determined by the mass, length, and pennation angle of the muscle (Herrel et al., 2008), and is correlated with the force production capability of the muscle (Leonard et al., 2021). PCSA is equal to the muscle volume (typically determined as muscle mass divided by a standard density for vertebrate skeletal muscle) divided by the fiber length (Santana, 2018). The higher the PCSA, the greater the force that is generated (high muscle volume, smaller fibers), in turn, the lower the PCSA the lower the force that is generated (lower muscle volume, larger fibers) (Leonard et al., 2021). Also, maximizing bite force with a muscle insertion on the jaw with angle near 90° is a contributing factor to a higher bite force, as force varies with the *sine* of this angle.

Cranial Bite Force Resistance

Cranial bite resistance and stress needs to be taken into consideration when looking at biomechanics of bite. Stress is the reaction of a physical object experiencing a force or “load”. There are two kinds of stress: normal and shear stress. Normal stress is calculated as the perpendicular force applied over the cross-sectional area of an object. For example, due to the external loading of bricks on a wall, the bricks will compress to sustain the weight. Shear stress is when there is parallel force applied onto the object (e.g., a wrecking ball applies shear stress to a brick wall). Stress can cause objects to deform or possibly break – for example, the breaking of a tooth when biting a hard food.

Skull shape plays a role in resistance as well (i.e., skull shape = form, stress resistance = function). Broad skulls with a shorter rostrum tend to handle a load more effectively than smaller, longer rostrums (Santana et al., 2012). Higher mechanical advantage and higher bite force may result in high stress on the skull without other associated shape adaptations to resist these high forces (Santana et al., 2012). Species with a shorter rostrum, larger skulls, and higher jaw moment obtain more shear stress (Santana et al., 2012). Skull stress may also vary with feeding behaviors. Individual bat species tend to favor a place in their mouth they prefer to chew (Dumont et al., 2005). These can vary from one to two teeth or unilateral (one-sided) bites to bilateral (two-sided) bites (Dumont et al., 2005). The stress resistance experience by different skull shapes were associated with mastication method in which they favored. This was supported by testing other forms of chewing and the preferred method deemed most fit (Dumont et al., 2005). It was also determined that there is more bending stress in deep

bilateral biting (Santana et al., 2012), and more torsional (twisting) in unilateral biting. Thus, different behaviours in bat biting will load differently across the cranium and jaw.

Bite Performance and Diet

Having a high bite force is an important performance trait and can increase the types of prey available for several bats (Shi et al., 2020). A high bite performance can lead to evolutionary divergence of cranial morphology by exploitation of different dietary specializations (frugivores, nectivores, insectivores, carnivores, piscivores, and sanguivores) (Arbour et al., 2019; Maestri et al., 2016; Santana & Cheung, 2016). Diets that contain bone, hard fruits, or hard insects (e.g., large beetles) rely on a greater force for consumption of prey compared to a nectivorous bat or insectivorous bat (especially diptera and lepidoptera specialists), which do not need as much force (Shi et al., 2020). Bird eating bats and carnivorous bats possess greater mechanical adaptations to account for the mastication of hard bones (Shi et al., 2020). Similarly, piscivorous bats have a high bite force (although not as strong as bird eating and carnivorous bats) (Shi et al., 2020). All three dietary specializations still have a higher bite force than insectivores (there are some exceptions like beetle-eating insectivores) (Shi et al., 2020). Nectivores require the lowest bite force out of all bats (Shi et al., 2020). Thus, variation of bite force may be related to hardness of prey and allows for more dietary diversity. An example of this is demonstrated in *Centurio senex* (Madrid-López et al., 2013). *Centurio senex* consumes hard fruits and seeds and is hypothesized to have a skull that is advantageous for eating hard foods (Madrid-López et al., 2013). Having a bite force necessary for the

consumption of seeds and resistant that force, allows these species to fill a specific niche when food is sparse.

Although the functional implications of shape variation like elongation have been well-studied in mammals in general and in bats in particular (Dumont et al., 2014; Santana et al., 2012), the biomechanical consequences of rostral flexion have not been examined. This is particularly true for oral-echolocating bats, as most biomechanical studies are conducted in the nasal-emitting family Phyllostomidae. The results as presented in Chapter 1 show that rostral flexion is an essential characteristic of bat cranial variation, that it was important to the early evolution of skull shape and was influenced by selection for echolocation mode. Finite element analysis (FEA) can be used to test if there is a difference in stress experienced across the skull associated with rostral flexion. FEA is an engineering software that determines quantitative stress across an object experiencing a load (Curtis et al., 2020; Dumont et al., 2005). To accurately test if extreme rostral flexion has any consequences associated with bite force resistance, a model of *Mormoops blainvillii*, a species with an extreme upwards angle of the rostrum ($\sim 75^\circ$) was used. I assume that functional trade-offs associated with rostral flexion will be most pronounced in this extreme morphology. To permit direct comparisons of the impact of reducing rostral flexion from *Mormoops*, I compared this with a warped version of the skull to the species *Murina leucogaster* ($\sim 132^\circ$). By geometrically warping the skull, other individual shape features can be controlled for, which in theory will help to isolate the functional consequences of rostral flexion in contrast with other morphological attributes. Using FEA, force was applied to the unilateral canine, bilateral

canine, unilateral molar, and bilateral molar to accurately represent different bite behaviors and strategies shown in bats (Dumont et al., 2005; Santana et al., 2012).

MATERIALS AND METHODS

Calculation of Bite Force

$$F_{out} = F_{act} * \sin \alpha * MA$$

The formula above was used to calculate bite force for FEA analysis. F_{act} is the physiological cross section area (PCSA) multiplied by the scalar value of 25 (N/cm²). PCSA was calculated as the muscle volume (muscle mass / density of 1.06 g/cm³) divided by the average fiber length of the muscle. Data on muscle mass and fiber lengths were taken from dissection work previously conducted by J. Arbour. Muscles were manually dissected from both sides of the head for the masseter, temporalis, lateral pterygoid and the zygomaticomandibularis. The wet mass of each muscle was taken in grams. The muscles were then placed in a bath of 10% sulfuric acid and placed in an oven at 70°C and checked every 10 minutes until the fibers began to separate. The muscles were rinsed in distilled water and covered in glycerin. The fibers were then gently teased apart using fine needles and photographed under a dissecting microscope on a gridded background. Alpha (α) is equal to the angle of insertion of each muscle on the jaw, which was measured in "Geomagic" software. Angle of insertion was calculated after manipulating the mandible of the skull to a 30° jaw opening, to mimic realistic positions during biting (Santana, 2016). I calculated PCSA and alpha for four major muscles responsible for the production of bite force - *temporalis*, *masseter*, *lateral pterygoid*, and *zygomaticomandibularis*. Mechanical advantage was calculated by ratio between the input lever length (joint to muscle attachment on the mandible) to the output

lever length (jaw joint to the tip of the relevant tooth). Mechanical advantage was calculated for two different bite positions: at the canine and first molar. After all forces were calculated per muscle with each tooth, the sum was taken and multiplied by 2 to encompass both sides of the jaw musculature.

FE Analysis

Two species were used in FE analysis, *Mormoops blainvillii* and *Murina leucogaster*. STL files were collected from previously published work (Arbour et al., 2019). *Mormoops* was used due to the extreme angle of rostral flexion and echolocation type (oral echolocator). Files with a large number of triangles (>1 million) and many small structures/imperfections may result in computational errors during FEA, therefore the *Mormoops blainvillii* STL was manually cleaned of all irregularities, holes, and small structures (e.g., processes in the nasal turbines, foramen on the rostrum, etc.) in Geomagic (Curtis et al., 2020; Dumont et al., 2005).

To have a lower rostral angle to compare stress to, *Murina leucogaster* was used to mathematically transform (warp) the cleaned *Mormoops* to form a new biologically feasible skull, using thin-plate spline interpolation (Bookstein, 1989). *Murina* is a typical oral echolocator belonging to a closely related family (but with a substantially less upturned rostrum), thus transformation is likely to produce a biologically feasible skull shape. Warping was accomplished using landmark data in Stratovan Checkpoint, to warp *Mormoops* closer to the rostral flexion observed in *Murina*; a setting of “50%” warping was used for analysis (Fig. 11). The STL meshes for the natural and warped *Mormoops* crania were transformed into a four-noded tetraheadral mesh using Strand7, comprised of

“bricks” representing the solid materials of the skull (as opposed to STLs which are surface meshes only). Published mechanical properties of cortical bone were applied to all bricks: Poissons ratio ($\nu = 0.3$) and Young’s modulus of 2.512×10^4 MPa (Curtis et al., 2020). I did not apply different material properties for tooth enamel, and thus stress on the teeth are likely to be overestimated. Each model (natural and warped) was subject to four different loads: unilateral canine, bilateral canine, unilateral molar, and bilateral molar. Three to four constraints were associated with each load; one constraint was located on each of the mandibular fossa, where the jaw articulates with the cranium. To avoid over constraining, one of the fossa was fixed in all directions and the other was fixed in two of the directions (Curtis et al., 2020; Dumont et al., 2005). Bite force was applied as to a single node at the tip of each tooth (either one or two teeth: canine or molar) as a static load.

Table 3. Summary of muscle measurements. MA = Mechanical Advantage, α = angle of insertion, and PCSA = physiological cross section area

	Muscle	MA	α	PCSA (cm²)
<i>Canine</i>	temporalis	0.2461	47.932	0.17802
	masseter	0.193357	37.562	0.03229
	lat. pterygoid	0.299352	34.884	0.00829
	zygomaticomandibularis	0.219192	36.018	0.01221
<i>Molar</i>	temporalis	0.341897	47.932	0.17802
	masseter	0.268624	37.562	0.03229
	lat. pterygoid	0.415878	34.884	0.00829
	zygomaticomandibularis	0.304514	36.018	0.01221

The temporalis and masseters have the highest contribution on bite force for both canine and molar bites, temporalis having the higher affect out of the two. Final forces applied to natural skull 1.9661 N for canine and 2.7314 N for molar for unilateral bites. Once corrected for size of models, force applied to the warped skull were 2.5582 N for canine and 3.5540 N for molar for unilateral bites. Half of these values were applied to each tooth for bilateral bites.

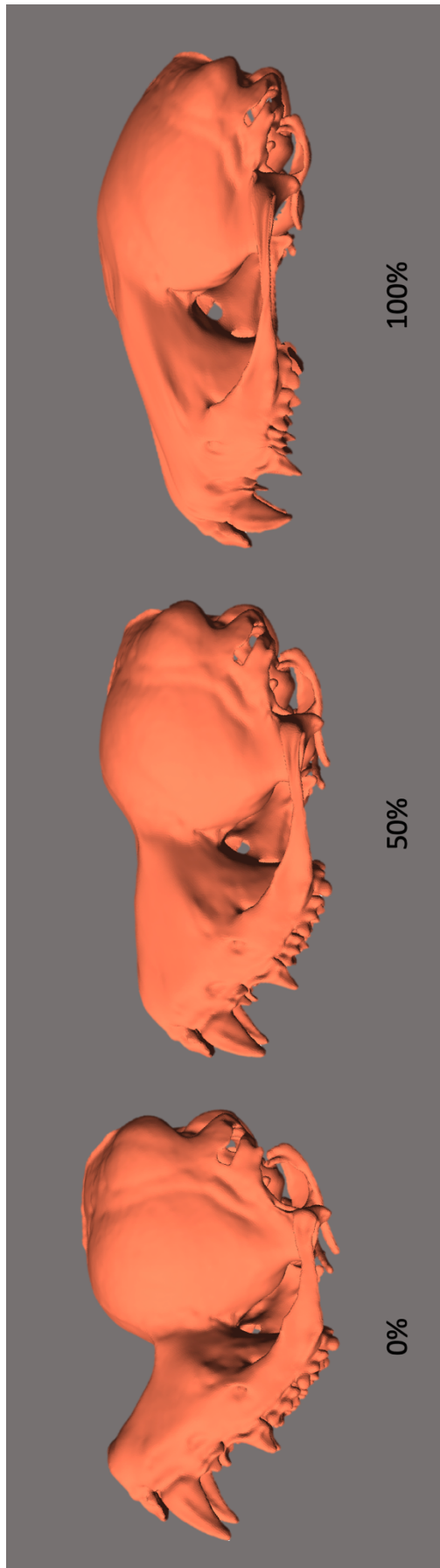


Figure 11. Natural and mathematically deformed (warped) *Mormoops* crania. 0% is *Mormoops blainvillii*. 50% is showing original *Mormoops* skull warped to be morphologically similar to *Murina leucogaster*. 100% is a fully warped *Mormoops* skull, note the features that are unnatural (i.e., teeth and bulgy lobes in the back of the skull).

To ensure that differences in stress were a result of only shape, the load applied to the warped skull was scaled to maintain a the same proportional surface area to force ratio as the natural skull (Dumont et al., 2009). The warped model had a surface area of 1023.0133 mm² and a volume of 98.187 mm³. The natural model had a surface area of 786.2265 mm² and a volume of 66.854 mm³. Muscle forces were scaled using the equation below:

$$F'_B = \left(\frac{SA_B}{SA_A} \right) F_A$$

F'_B is the new force needed for the new models, which was calculated by the warped surface area (SA_B) divided by the natural surface area(SA_A), then its multiplied by the force of the natural skull (F_A) (Dumont et al., 2009). Using Strand7 I determined the Von Mises stress (MPa) across the bricks in each model given the load and constraints applied. I compared the resulting median and range of stress values observed in the rostrum and braincase (see Fig. 12) in the natural and warped skulls across each of the four loading scenarios (Fig. 12). I excluded very high stress values associated with the loading points, which in these FEA models are represented as single point nodes on the surface of the model, by expressing the 99th percentile of stress values rather than the maximum (henceforth referred to as “peak” stresses).

Due to the resulting stress data being skewed, a non-parametric test was used to find if there was a difference between the statistical distributions of stress of the rostrum and braincase/zygomatics in the natural and warped skulls. The skull was divided into two halves and the data was collected for the rostrum (selected) and the braincase/

zygomatics (unselected) (Fig. 12). In R Statistical Package, multiple Mann Whitney U tests were completed by comparison of the natural and warped skulls for each of the rostrum and braincase of each FEA simulation (the results are shown in Table 4). I applied a Holm-Bonferroni correction for multiple comparisons to the significance of each test.

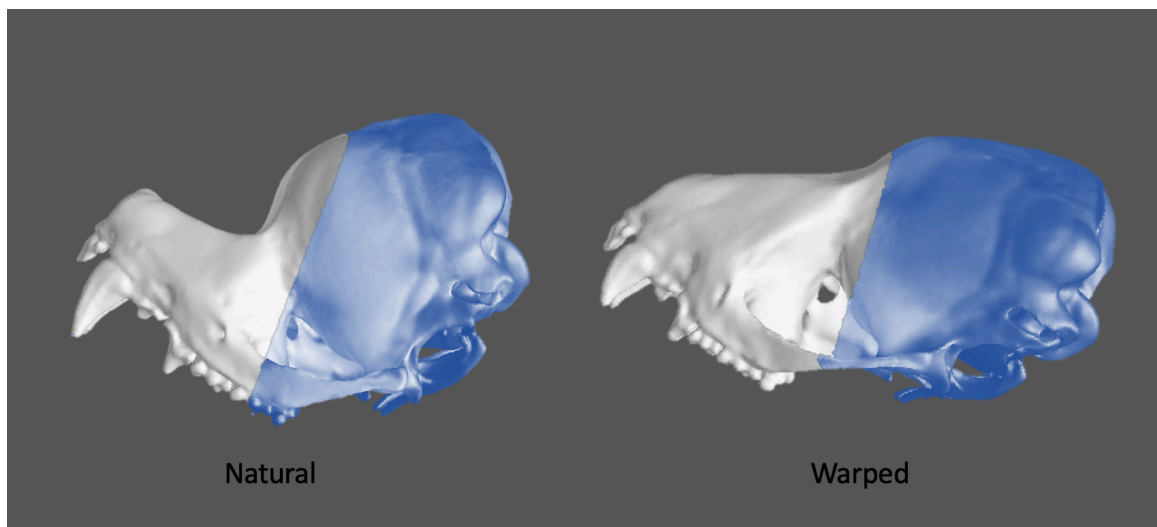


Figure 12. Shows area of selected (white), classified as rostrum and unselected, the braincase/zygomatics (colored) of natural and warped skulls.

RESULTS

Across both the natural and warped skulls, stress was lower for bilateral bites (compared to unilateral) and for molar bites (compared to canine bites). However, within specific biting behaviors I observed differences between the warped and natural skulls. Stress values were significantly higher in the natural skull in the cases of the **unilateral canine bite**, in both the rostrum and braincase region (Table 4). In the case of a unilateral canine bite, median stress was 12% higher in the rostrum and 56% higher in the braincase of the natural skull. High peak stress values (99th percentile values) were similarly elevated in the natural skull (Table 4). The ratio of stress between the rostrum and braincase was lower in the natural skull (2.14×) than the warped skull (3.01×), indicating that stress was not only higher but more dispersed in the natural skull.

The distribution of stress is shown to be greater on the dorsal inflexion point of the rostrum (i.e., its connection to the braincase) as compared to the rest of the natural skull (Fig. 13) The radiation of the force seems to disperse high stress across the entirety of the natural skull while the warped skull has a more centralized stress surrounding the bite itself. Interestingly, a higher stress was associated with the left zygomatic (side in which force was applied) in the warped skull as compared to the natural skull. Although, the natural skull seems to have a higher force on the right zygomatic. In both the natural and the warped skulls, the rostrum obtains a higher stress than the basicranium/zygomatics (Table 4).

Both the **bilateral canine bite** and **bilateral molar bite** show similar patterns,—the natural skull shows significantly lower stress values in both the rostrum and braincase, as well as lower peak stress in the braincase. However, in both cases the

rostrum of the natural skull experiences higher peak stresses than the warped skull. In the **bilateral canine bite** differences in median stress were trivial; 1.5% higher in the rostrum and 0.7% higher in the braincase in the warped skull. However, peak stress was 19% higher in the rostrum of the natural skull, and 22% higher in the braincase of the warped skull. The rostrum of the natural skull in particular seems to have a high stress in a more concentrated area running from the base of the canine dorsoposteriorly to the inflection of the rostrum and the braincase. Therefore, even though the median stress is similar between the two skulls, in the warped skull the force distributes across the rostrum more effectively (Fig. 14). The zygomatics have spots of higher stress compared to the rest of the brain case but there is a high stress concentrated on the ventral surface of the braincase surrounding the pterygoid hamulus attachment.

In a **unilateral molar bite**, the stress in the rostrum has no statistical difference between warped and natural skulls (Table 4, $W= 1.35 \times 10^{11}$, $p>0.05$). However, the braincase/zygomatics have significantly higher stress in the natural skull than the warped skull (Table 4, $W=3.77 \times 10^{11}$, $p < 0.05$). Median stress in the braincase was 65% higher in the natural skull, though peak stress was 8% higher in the warped skull. The natural skull appears to have more widespread distribution of elevated stress throughout the entirety of the skull while on the warped skull the stress stays centralized around the loading point on the left side of the skull and around the inflection point of the rostrum. This pattern is also seen in the hard palate (more extensive “green” areas in the ventral view of the natural skull, Fig. 15). The zygomatic arches and braincase also have noticeably higher stress in the natural than the warped.

In the **bilateral molar bite**, the stress was significantly higher in the warped skull in both the rostrum and the braincase/zygomatrics (Table 4). Median stress was 25% higher in rostrum and 46% higher in the braincase of the warped skull. Both skulls have the stress aggregated around the inflexion point of the rostra (Fig. 16). The warped skull has a higher stress on the zygomatrics and a higher distribution of the stress on the basicranium and other ventral surfaces.

Table 4. Summary of Median stress, 1st and 3rd quantiles of stress, 99th percentile of stress and results of Mann Whitney U test. Lowest numbers in the pair are bolded.

Force Applied	Model	Region	Stress Median	Stress (Q1, Q3)	99th Percentile	Mann Whitney W	Mann Whitney P-value
Unilateral Canine	Natural	Rostrum	0.407275	0.1399,0.9631	5.13376	1.73 x 10 ¹¹	< 2.20 x 10 ⁻¹⁶
	Warped	Rostrum	0.3645	0.1294,0.8093	4.31342		
	Natural	Braincase/Zygomatic	0.1898785	0.06235,0.49811	2.72704	3.39 x 10 ¹¹	< 2.20 x 10 ⁻¹⁶
	Warped	Braincase/Zygomatic	0.12127	0.04056, 0.29270	2.43322		
Bilateral Canine	Natural	Rostrum	0.346952	0.1323 , 0.7460	3.24057	1.40 x 10 ¹¹	7.89 x 10 ⁻¹⁶
	Warped	Rostrum	0.3524	0.1400, 0.5258	2.70937		
	Natural	Braincase/Zygomatic	0.10582	0.03266,0.30515	1.92651	3.11 x 10 ¹¹	< 2.20 x 10 ⁻¹⁶
	Warped	Braincase/Zygomatic	0.1066	0.03866, 0.27560	2.36285		
Unilateral Molar	Natural	Rostrum	0.2666	0.0838,0.6674	3.97257	1.35 x 10 ¹¹	0.789
	Warped	Rostrum	0.2632	0.0934, 0.6170	4.32999		
	Natural	Braincase/Zygomatic	0.2372	0.077,0.5944	3.21876	3.77 x 10 ¹¹	< 2.20 x 10 ⁻¹⁶
	Warped	Braincase/Zygomatic	0.14313	0.04983, 0.36871	2.74679		
Bilateral Molar	Natural	Rostrum	0.18568	0.06353,0.44238	2.25018	1.23 x 10 ¹¹	< 2.20 x 10 ⁻¹⁶
	Warped	Rostrum	0.23276	0.08446,0.51363	2.21264		
	Natural	Braincase/Zygomatic	0.05834	0.01798,0.16830	1.32129	2.78 x 10 ¹¹	< 2.20 x 10 ⁻¹⁶
	Warped	Braincase/Zygomatic	0.0852	0.03036, 0.22894	1.70588		

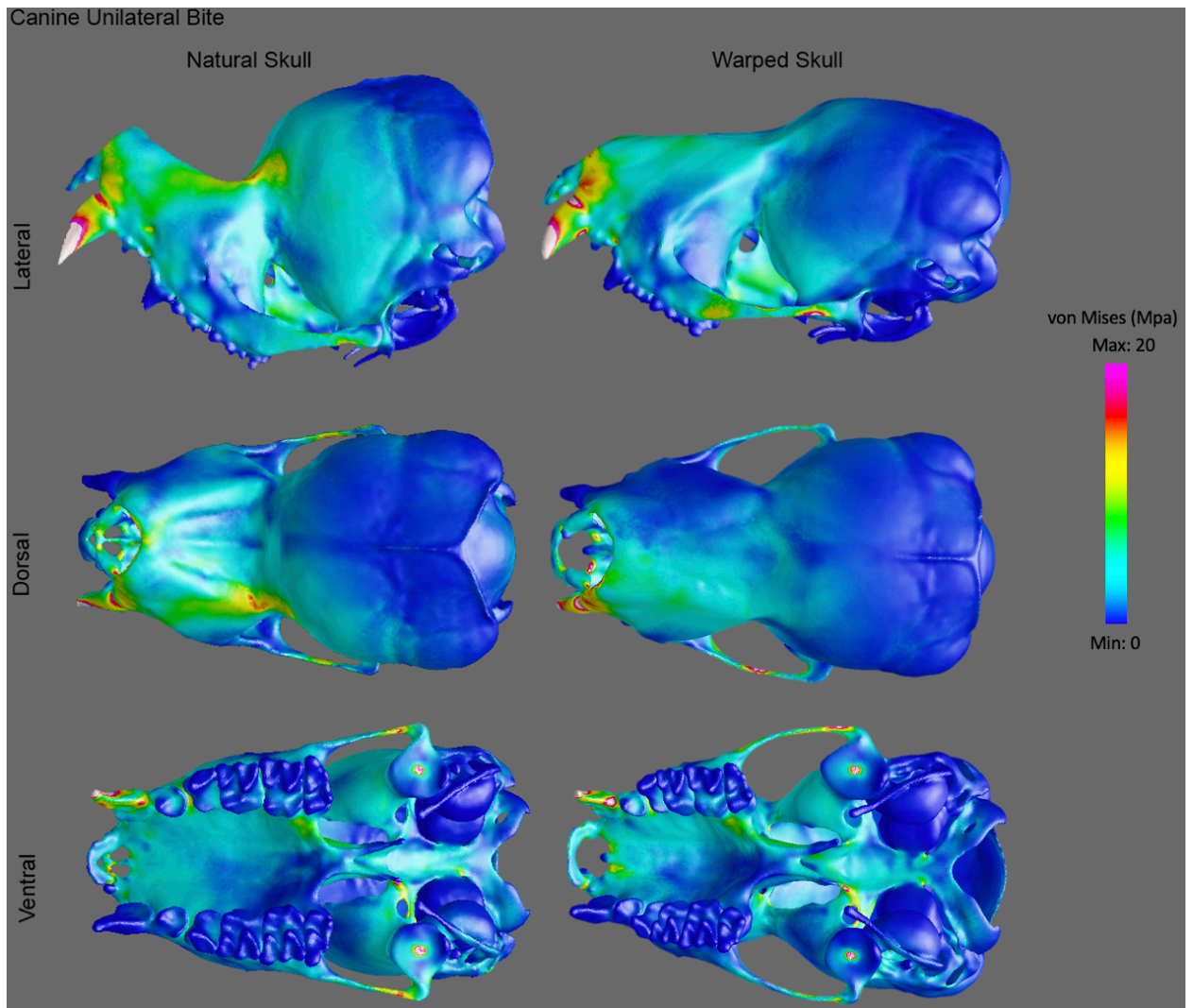


Figure 13. Stress distribution across two skulls (natural and warped) from a canine unilateral bite.

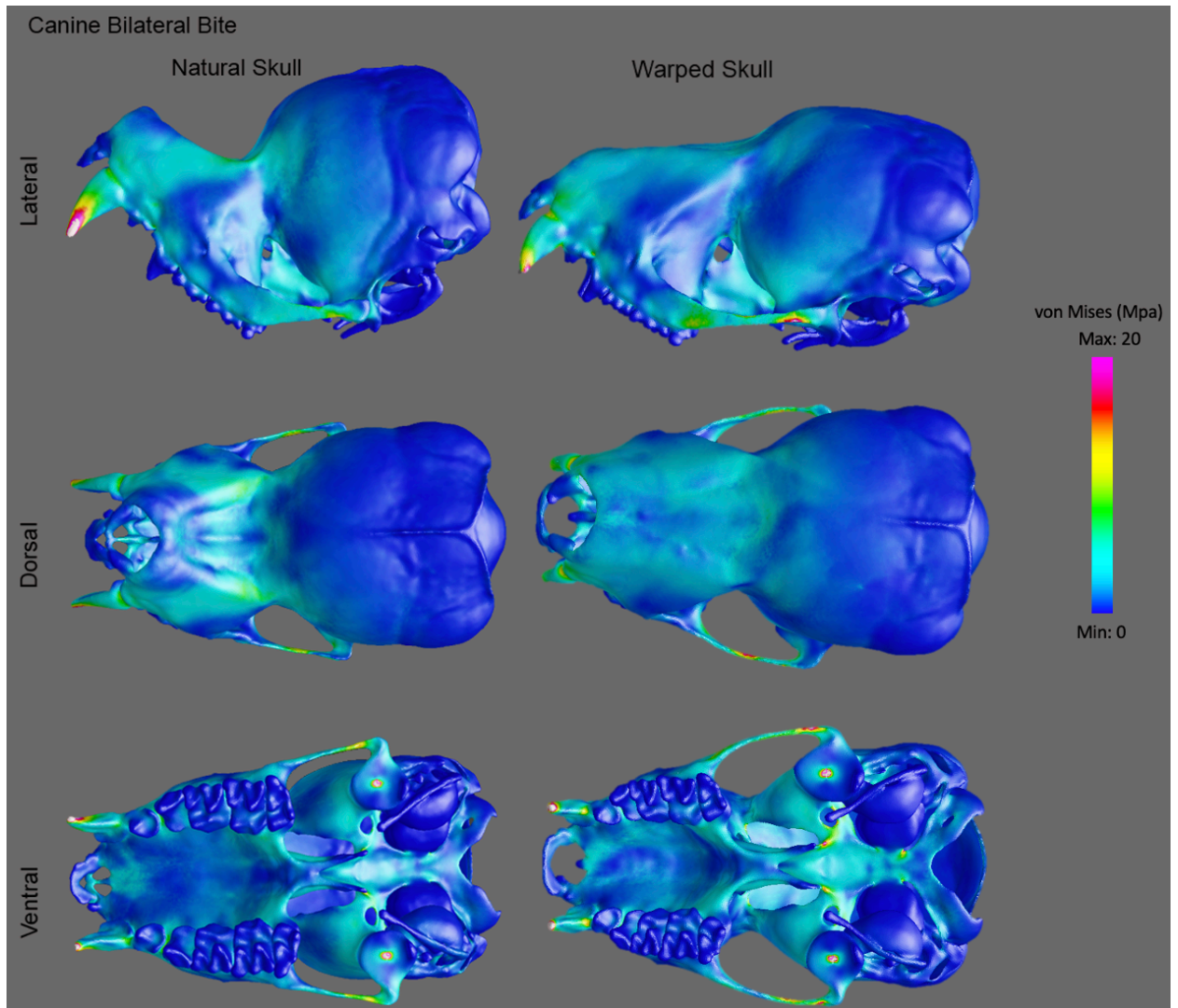


Figure 14. Stress distribution across two skulls (natural and warped) from a canine bilateral bite.

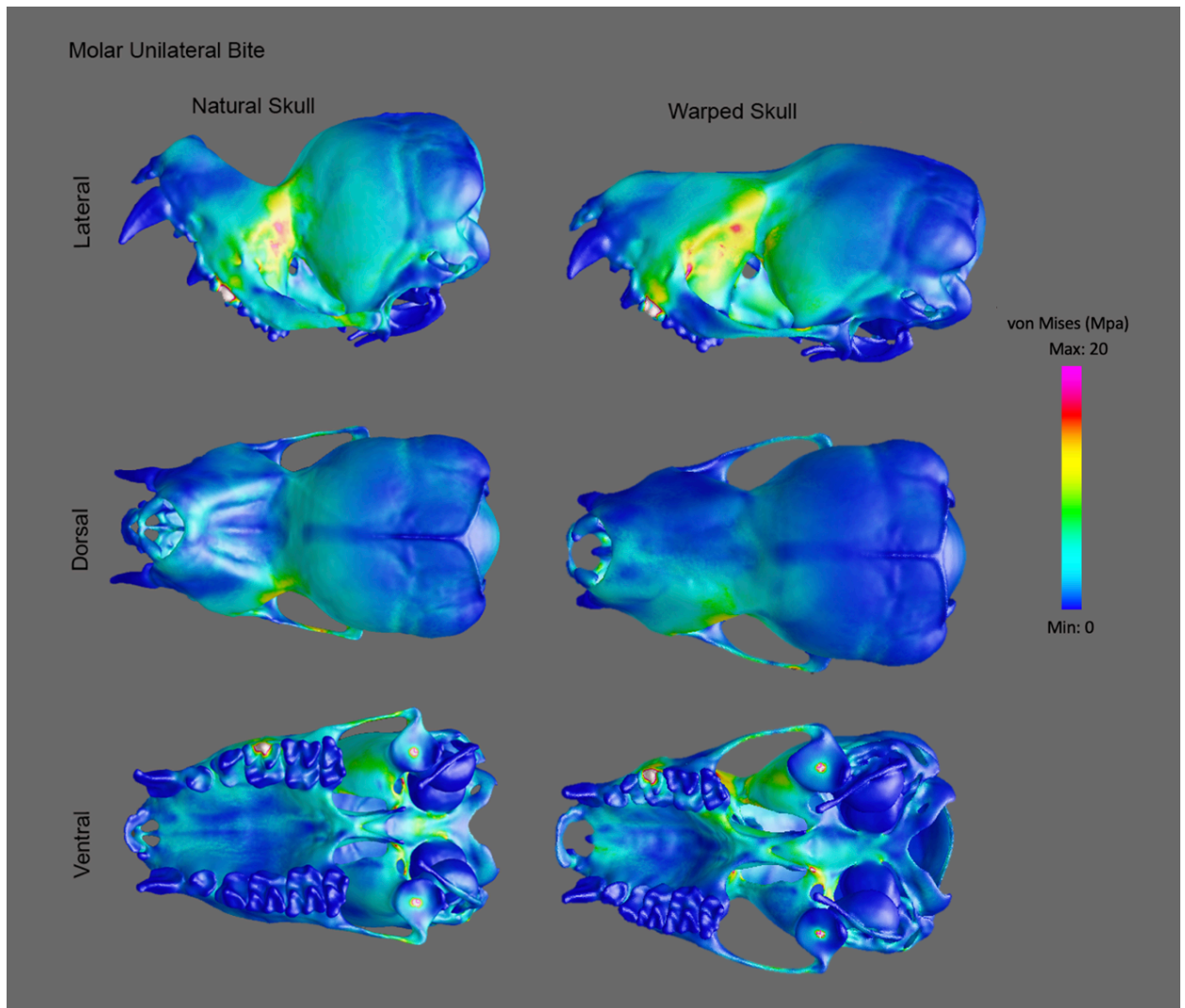


Figure 15. Stress distribution across two skulls (natural and warped) from a molar unilateral bite.

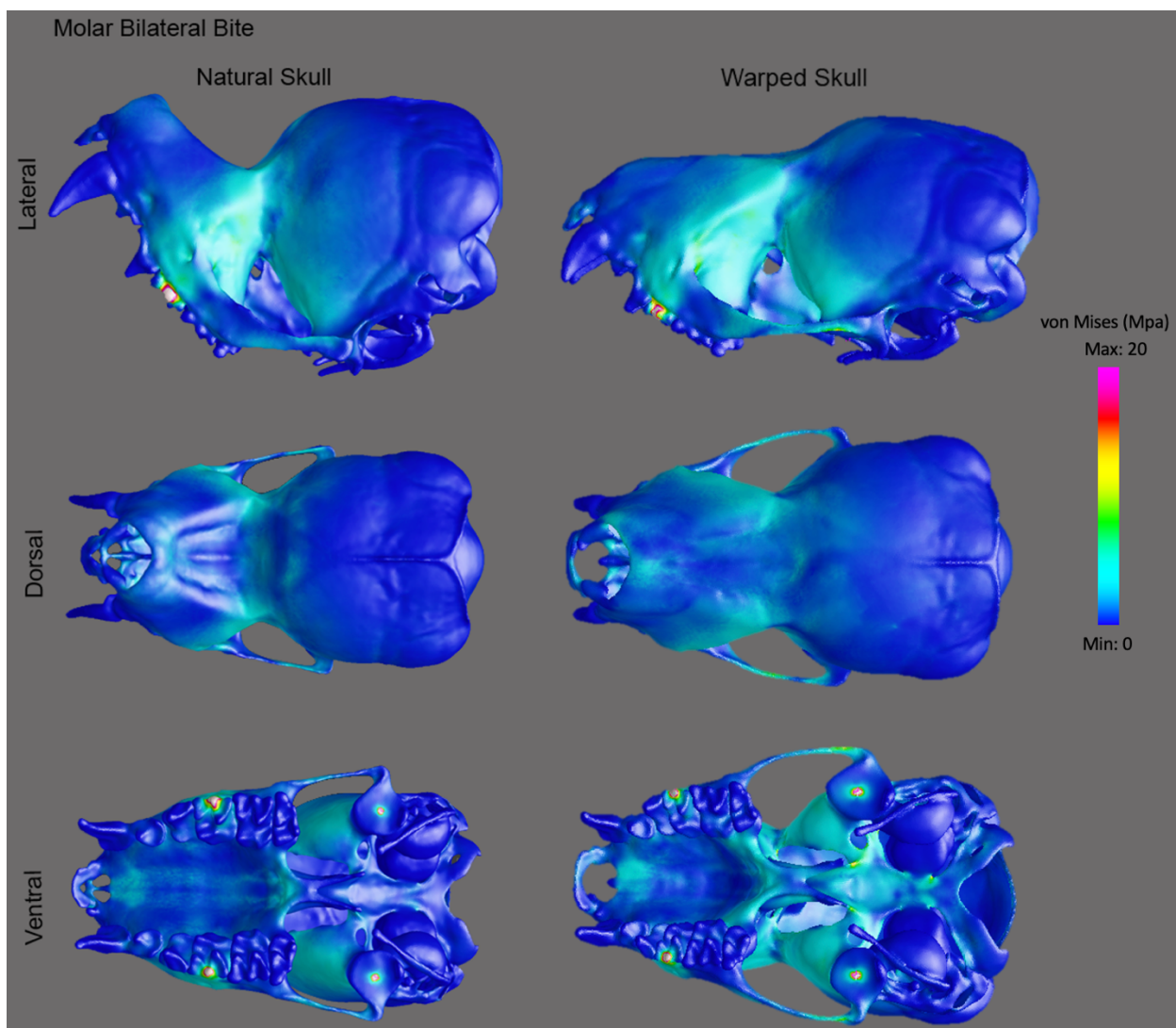


Figure 16. Stress distribution across two skulls (natural and warped) from a molar bilateral bite.

DISCUSSION

The study of form in relation to function is important to understanding how organisms adapt to their environment, and how this connects to their developmental processes. The diversity of bat skulls has been at least partly shaped by evolutionary pressures associated with echolocation, especially in the evolution of trait morphology related to rostral flexion (see Chapter 1 and Arbour et al., 2019). Our work in this chapter demonstrates that there are significant biomechanical consequences to rostral flexion relating to the distribution and resistance to bite force. Overall, the model with a more upturned snout tends to show less effective dispersal of bite forces, and frequently higher stress across the skull. However, the biomechanical implications of rostral flexion appear to vary with biting behaviors. For example, the upturned rostra associated with the natural *Mormoops* skull show reduced median stress in bilateral molar bites compared to the warped skull with reduced rostral flexion. In general, however, selection for high rostral flexion associated with oral echolocator appears to be associated with a biomechanical trade-off in the crania's ability to resist strong bite forces.

Interestingly, some oral emitters that eat harder prey, such as beetles (*Nyctalus*), tend to have a more upturned rostrum. Individuals with a more upturned rostrum tend to have shorter crania and possessing this trait may produce a higher mechanical advantage compensating for capability to consume the harder prey. Also, these bats may participate in bilateral biting that was found to possess a higher resistance for bite force than unilateral biting. Conversely, other beetle eaters (Molossid and *Eptesicus fuscus*), have relatively more downturn rostra (~140°, 116°, respectively) which are able to resist higher bite forces for unilateral bites. Individuals with a more elongate skull tend to have

a more average to downturn rostrum and a lower mechanical advantage, although, these skulls tend to have musculature more effective for mastication.

There are several physiological ways that bite force can be increased (see below), but there are also several behavioral ways that bats have been observed to increase their bite force. One way to increase bite force is that some tend to move their food closer to the back of the jaw joint (especially hard foods) (Santana et al., 2012). This moves the food to a region of higher mechanical advantage, where greater force from the jaw muscles may be transmitted (Santana, 2016). Moving from a bilateral to unilateral bite is also frequently observed in Phyllostomid species feeding on harder foods (Santana & Dumont, 2009). Unilateral bites in particular showed the most negative impacts on stress distribution in *Mormoops*, though the impact was more limited in unilateral molar bites.

There are several differences present in the bite force distribution across the skull of an extreme upturned rostrum and a more average angle of rostrum. As seen in table 4, the unilateral bites tend to have a higher stress associated with the entire skull of the natural rostral angle and the bilateral bites have a higher stress in the warped skulls. With this being said, there might be a higher risk of shear stress with unilateral bites than bilateral in extreme rostral flexion. *Mormoopidae* may favor bilateral bites versus unilateral bites but may restrict the initial capture of prey. Insectivorous bats are found to use their canine teeth to capture prey, bilaterally or unilaterally (Curtis et al., 2020), thus restricting venturing into harder prey items. Although, the natural skull was found to have a lower stress in the rostrum than in the warped, in canine bilateral bite, the stress of the bite was highly aggregated around the rostrum while the stress on the warped skull was more evenly distributed across the skull. An even distribution of stress may reduce the

shear associated with the bite force itself and could have a higher potential to take on more complex diets. As for molar unilateral bites, the natural skull force was greatly distributed across the skull, most particularly in the flexion of the rostrum. Compared to the warped skull, that had a lower distribution of stress across the skull and a lower amount of stress associated with the flexion of the rostrum. With this, developing a more extreme upturn snout possess a functional tradeoff for a more accurate emission of echolocation but a lower capability of dietary diversity.

It is important to note that, outside of the region the load was applied to the teeth, the stress observed in both the natural and warped skull models was well below the limit where major bone fractures could occur (~ 140 MPa in cortical bone) (Dumont et al., 2005). The method used to estimate bite force here has been shown to be well correlated with observed bite force values in bats, but may underestimate bite force (Santana et al., 2010). But it is unlikely bite force would be sufficiently underestimated to impact this conclusion. However, long term stress on bones may cause “fatigue” and compromise the ability of bones to resist subsequent shear stress even at low stress/strain values (Dumont et al., 2005). Thus, occasional use of very strong bites may be tolerated even in species with strongly upturned skulls, while very regular use for durophagus diets may be more detrimental to bone health.

Insectivorous phyllostomids were shown to be less likely to vary their biting behaviors in a response to different diets in a previous study (Santana & Dumont, 2009). Because phyllostomids obtain a relatively higher rostral flexion (mean = 148.37°) than oral echolocators (mean = 122.99°), the lower rostral flexion allows for a higher diversity

of diet due to the capacity to withstand greater stress. Therefore, extreme rostral flexion may not be able to handle foods with a higher resistance.

This study does not account for other morphological features that may help to compensate for the changes in force distribution within the skull. Tooth type has an influence on bite force (Santana et al., 2010). Molars have a higher bite force than incisors, because they have a higher mechanical advantage further back in the jaw (Santana et al., 2010). Bats may also use changes in size to escape some of these limitations on bite force resistance observed in oral emitters. Carnivory for example was more strongly associated with head size than with skull shape, with the exception of species feeding on fish (Santana & Cheung, 2016). Interestingly, the bird-eating *Nyctalus noctula* which shows a fairly upturned snout, is a large bat among oral-emitters, especially compared with its more exclusively dipteran feeding congeners. Cleft palates are also commonly found in bats and are associated with reductions in the ability to resist forces. They occur repeatedly, likely through similar developmental mechanisms, but their size and impact on bite force resistance varies across oral emitters. There are likely cases in which there are selection on other aspect of skull function. Although rostral flexion constraints dietary diversity, the flexion itself may be more effective for oral emission, or a larger gape evolved as a mechanism for larger prey capture. Thus having a skull more suited for prey capture and echolocation mechanisms may be more important than consumption of prey (Freeman, 1984).

CONCLUSION

Selection for an upturned rostral flexion may limit future adaptive opportunities for oral emitters. By reducing resistance to force, an upturned rostral flexion restricts the capability to venture into new dietary niches, due to the more complex prey. Although, an upturn rostrum may be more effective for other functional trade-offs such as, larger gape for prey manipulation and better oral emission. According to our results, more downturn rostrums may experience a higher fitness associated with an increased capability to explore a more varied diet. However more in-depth analysis will need to be performed to examine biomechanical consequences of extremely downturned skulls and their functional trade-offs (i.e., nasal domes and floating premaxilliae). Given the strong reliance on nasal-emitters for biomechanical studies of bite force in bats, this work also illustrates a need for a greater focus on oral-emitters in understanding the evolution of form and function trends across a greater diversity of bats.

REFERENCES

- Arbour, J. H., Curtis, A. A., & Santana, S. E. (2021). Sensory adaptations reshaped intrinsic factors underlying morphological diversification in bats. *BMC Biology*, *19*(1), 1–13. <https://doi.org/10.1186/s12915-021-01022-3>
- Arbour, Jessica H., & Brown, C. M. (2014). Incomplete specimens in geometric morphometric analyses. *Methods in Ecology and Evolution*, *5*(1), 16–26. <https://doi.org/10.1111/2041-210X.12128>
- Arbour, Jessica H., Curtis, A. A., & Santana, S. E. (2019). Signatures of echolocation and dietary ecology in the adaptive evolution of skull shape in bats. *Nature Communications*, *10*(1). <https://doi.org/10.1038/s41467-019-09951-y>
- Beaulieu, J. M., Jhwueng, D. C., Boettiger, C., & O’Meara, B. C. (2012). Modeling stabilizing selection: Expanding the Ornstein-Uhlenbeck model of adaptive evolution. *Evolution*, *66*(8), 2369–2383. <https://doi.org/10.1111/j.1558-5646.2012.01619.x>
- Bollback, J. P. (2006). SIMMAP: Stochastic character mapping of discrete traits on phylogenies. *BMC Bioinformatics*, *7*, 1–7. <https://doi.org/10.1186/1471-2105-7-88>
- Bookstein, F. L. (1989). Principal Warps: Thin-Plate Splines and the Decomposition of Deformations. In *IEEE Transactions on Pattern Analysis and Machine Intelligence* (Vol. 11, Issue 6, pp. 567–585). <https://doi.org/10.1109/34.24792>
- Collar, D. C., O’Meara, B. C., Wainwright, P. C., & Near, T. J. (2009). Piscivory limits diversification of feeding morphology in centrarchid fishes. *Evolution*, *63*(6), 1557–1573. <https://doi.org/10.1111/j.1558-5646.2009.00626.x>
- Collyer, M. L., Sekora, D. J., & Adams, D. C. (2015). A method for analysis of

- phenotypic change for phenotypes described by high-dimensional data. *Heredity*, *115*(4), 357–365. <https://doi.org/10.1038/hdy.2014.75>
- Colombo, M., Damerou, M., Hanel, R., Salzburger, W., & Matschiner, M. (2015). Diversity and disparity through time in the adaptive radiation of Antarctic notothenioid fishes. *Journal of Evolutionary Biology*, *28*(2), 376–394. <https://doi.org/10.1111/jeb.12570>
- Curtis, A. A., Arbour, J. H., & Santana, S. E. (2020). Mind the gap: Natural cleft palates reduce biting performance in bats. *Journal of Experimental Biology*, *223*(2). <https://doi.org/10.1242/jeb.196535>
- Curtis, A. A., & Simmons, N. B. (2017). Unique Turbinal Morphology in Horseshoe Bats (Chiroptera: Rhinolophidae). *Anatomical Record*, *300*(2), 309–325. <https://doi.org/10.1002/ar.23516>
- Dean, A., Collyer, M., Baken, E., & Adams, M. D. (2022). Package ‘geomorph.’
- Dumont, E. R., Grosse, I. R., & Slater, G. J. (2009). Requirements for comparing the performance of finite element models of biological structures. *Journal of Theoretical Biology*, *256*(1), 96–103. <https://doi.org/10.1016/j.jtbi.2008.08.017>
- Dumont, Elizabeth R., Dávalos, L. M., Goldberg, A., Santana, S. E., Rex, K., & Voigt, C. C. (2012). Morphological innovation, diversification and invasion of a new adaptive zone. *Proceedings of the Royal Society B: Biological Sciences*, *279*(1734), 1797–1805. <https://doi.org/10.1098/rspb.2011.2005>
- Dumont, Elizabeth R., Piccirillo, J., & Grosse, I. R. (2005). Finite-element analysis of biting behavior and bone stress in the facial skeletons of bats. *Anatomical Record - Part A Discoveries in Molecular, Cellular, and Evolutionary Biology*, *283*(2), 319–

330. <https://doi.org/10.1002/ar.a.20165>

Dumont, Elizabeth R., Samadevam, K., Grosse, I., Warsi, O. M., Baird, B., & Davalos, L.

M. (2014). Selection for mechanical advantage underlies multiple cranial optima in new world leaf-nosed bats. *Evolution*, *68*(5), 1436–1449.

<https://doi.org/10.1111/evo.12358>

Feilich, K. L., & López-Fernández, H. (2019). When Does Form Reflect Function?

Acknowledging and Supporting Ecomorphological Assumptions. *Integrative and Comparative Biology*, *59*(2), 358–370. <https://doi.org/10.1093/icb/icz070>

Freeman, P. W. (1984). Functional cranial analysis of large animalivorous bats

(Microchiroptera). *Biological Journal of the Linnean Society*, *21*(4), 387–408.

<https://doi.org/10.1111/j.1095-8312.1984.tb01601.x>

Gunz, P., Mitteroecker, P., Neubauer, S., Weber, G. W., & Bookstein, F. L. (2009).

Principles for the virtual reconstruction of hominin crania. *Journal of Human Evolution*, *57*(1), 48–62. <https://doi.org/10.1016/j.jhevol.2009.04.004>

Herrel, A., De Smet, A., Aguirre, L. F., & Aerts, P. (2008). Morphological and

mechanical determinants of bite force in bats: Do muscles matter? *Journal of Experimental Biology*, *211*(1), 86–91. <https://doi.org/10.1242/jeb.012211>

Jones, G. (2009). Echolocation. *Encyclopedia of Marine Mammals*, *15*(13), 348–357.

<https://doi.org/10.1016/B978-0-12-373553-9.00085-7>

Jones, G., & Teeling, E. C. (2006). The evolution of echolocation in bats. *Trends in*

Ecology and Evolution, *21*(3), 149–156. <https://doi.org/10.1016/j.tree.2006.01.001>

Klingenberg, C. P. (2014). Studying morphological integration and modularity at

multiple levels: Concepts and analysis. *Philosophical Transactions of the Royal*

Society B: Biological Sciences, 369(1649), 33–35.

<https://doi.org/10.1098/rstb.2013.0249>

Kraatz, B., & Sherratt, E. (2016). Evolutionary morphology of the rabbit skull. *PeerJ*, 2016(9), 1–23. <https://doi.org/10.7717/peerj.2453>

Larouche, O., Hodge, J. R., Alencar, L. R. V, Camper, B., Adams, D. S., Zapfe, K., Friedman, S. T., Wainwright, P. C., & Price, S. A. (2020). Do key innovations unlock diversification? A case-study on the morphological and ecological impact of pharyngognathy in acanthomorph fishes. *Current Zoology*, 66(5), 575–588.

<https://doi.org/10.1093/cz/zoaa048>

Leiser-Miller, L. B., & Santana, S. E. (2021). Functional differences in echolocation call design in an adaptive radiation of bats. *Ecology and Evolution*, 11(22), 16153–16164. <https://doi.org/10.1002/ece3.8296>

Leonard, K. C., Worden, N., Boettcher, M. L., Dickinson, E., Omstead, K. M., Burrows, A. M., & Hartstone-Rose, A. (2021). Anatomical and ontogenetic influences on muscle density. *Scientific Reports*, 11(1), 1–11. <https://doi.org/10.1038/s41598-021-81489-w>

Madrid-López, S. M., Castro-Luna, A. A., & Galindo-González, J. (2013). First report of a hard fruit in the diet of *Centurio senex* (Chiroptera: Phyllostomidae) in Mexico. *Journal of Mammalogy*, 94(3), 628–631. <https://doi.org/10.1644/12-MAMM-A-218.1>

Maestri, R., Patterson, B. D., Fornel, R., Monteiro, L. R., & de Freitas, T. R. O. (2016). Diet, bite force and skull morphology in the generalist rodent morphotype. *Journal of Evolutionary Biology*, 29(11), 2191–2204. <https://doi.org/10.1111/jeb.12937>

- Pedersen, S. C. (1998). Morphometric analysis of the chiropteran skull with regard to mode of echolocation. *Journal of Mammalogy*, 79(1), 91–103.
<https://doi.org/10.2307/1382844>
- Rossoni, D. M., Assis, A. P. A., Giannini, N. P., & Marroig, G. (2017). Intense natural selection preceded the invasion of new adaptive zones during the radiation of New World leaf-nosed bats. *Scientific Reports*, 7(1), 1–11.
<https://doi.org/10.1038/s41598-017-08989-6>
- Santana, S. E., & Dumont, E. R. (2009). Connecting behaviour and performance: The evolution of biting behaviour and bite performance in bats. *Journal of Evolutionary Biology*, 22(11), 2131–2145. <https://doi.org/10.1111/j.1420-9101.2009.01827.x>
- Santana, Sharlene E. (2016). Quantifying the effect of gape and morphology on bite force: Biomechanical modelling and in vivo measurements in bats. *Functional Ecology*, 30(4), 557–565. <https://doi.org/10.1111/1365-2435.12522>
- Santana, Sharlene E. (2018). Comparative Anatomy of Bat Jaw Musculature via Diffusible Iodine-Based Contrast-Enhanced Computed Tomography. *Anatomical Record*, 301(2), 267–278. <https://doi.org/10.1002/ar.23721>
- Santana, Sharlene E., & Cheung, E. (2016). Go big or go fish: Morphological specializations in carnivorous bats. *Proceedings of the Royal Society B: Biological Sciences*, 283(1830). <https://doi.org/10.1098/rspb.2016.0615>
- Santana, Sharlene E., Dumont, E. R., & Davis, J. L. (2010). Mechanics of bite force production and its relationship to diet in bats. *Functional Ecology*, 24(4), 776–784.
<https://doi.org/10.1111/j.1365-2435.2010.01703.x>
- Santana, Sharlene E., Grosse, I. R., & Dumont, E. R. (2012). Dietary hardness, loading

behavior, and the evolution of skull form in bats. *Evolution*, 66(8), 2587–2598.

<https://doi.org/10.1111/j.1558-5646.2012.01615.x>

Shi, B., Wang, Y., Gong, L., Chang, Y., Liu, T., Zhao, X., Lin, A., Feng, J., & Jiang, T.

(2020). Correlation of skull morphology and bite force in a bird-eating bat (*Ia io*;

Vespertilionidae). *Frontiers in Zoology*, 17(1), 1–14.

<https://doi.org/10.1186/s12983-020-00354-0>

Slater, G. J., Price, S. A., Santini, F., & Alfaro, M. E. (2010). Diversity versus disparity

and the radiation of modern cetaceans. *Proceedings of the Royal Society B:*

Biological Sciences, 277(1697), 3097–3104. <https://doi.org/10.1098/rspb.2010.0408>

Thiagavel, J., Cechetto, C., Santana, S. E., Jakobsen, L., Warrant, E. J., & Ratcliffe, J. M.

(2018). Auditory opportunity and visual constraint enabled the evolution of

echolocation in bats. *Nature Communications*, 9(1). [https://doi.org/10.1038/s41467-](https://doi.org/10.1038/s41467-017-02532-x)

[017-02532-x](https://doi.org/10.1038/s41467-017-02532-x)

Zelditch, M., Swiderski, D., Sheets, H., & Fink, W. (2004). Geometric Morphometrics

for Biologists. *Geometric Morphometrics for Biologists*, 1–443.

<https://doi.org/10.1016/B978-0-12-778460-1.X5000-5>

SUPPLEMENTARY MATERIALS

1. All 235 species with echolocation type, diet, family, added individuals, and angle of rostrum flexion.

<i>Aethalops alecto</i>	Non	frugivore	Pteropodidae	139.879521
<i>Ametrida centurio</i>	Nasal	frugivore	Phyllostomidae	163.126521
<i>Anoura caudifer</i>	Nasal	nectarivore	Phyllostomidae	135.186037
<i>Anoura geoffroyi</i>	Nasal	nectarivore	Phyllostomidae	131.87081
<i>Antrozous dubiaquercus</i>	Oral	insectivore	Vespertilionidae	119.843745
<i>Antrozous pallidus</i>	Oral	insectivore	Vespertilionidae	134.900305
<i>Artibeus hartii</i>	Nasal	frugivore	Phyllostomidae	148.830015
<i>Artibeus jamaicensis</i>	Nasal	frugivore	Phyllostomidae	153.384085
<i>Aselliscus tricuspidatus</i>	Nasal	insectivore	Hipposideridae	164.855368
<i>Balantiopteryx io</i>	Oral	insectivore	Emballonuridae	142.361054
<i>Balantiopteryx plicata</i>	Oral	insectivore	Emballonuridae	136.70536
<i>Balionycteris maculata</i>	Non	frugivore	Pteropodidae	139.82496
<i>Barbastella barbastellus</i>	Oral	insectivore	Vespertilionidae	124.422021
<i>Barbastella leucomelas</i>	Oral	insectivore	Vespertilionidae	132.442005
<i>Cardioderma cor</i>	Nasal	carnivorous	Megadermatidae	153.824255
<i>Carollia brevicauda</i>	Nasal	frugivore	Phyllostomidae	147.129646
<i>Carollia perspicillata</i>	Nasal	frugivore	Phyllostomidae	150.582444
<i>Centronycteris centralis</i>	Oral	insectivore	Emballonuridae	135.692645
<i>Centronycteris maximiliani</i>	Oral	insectivore	Emballonuridae	140.235597
<i>Centurio senex</i>	Nasal	frugivore	Phyllostomidae	156.336894
<i>Chaerephon leucogaster</i>	Oral	insectivore	Molossidae	130.983236
<i>Chaerephon pumilus</i>	Oral	insectivore	Molossidae	132.706516
<i>Chiroderma villosum</i>	Nasal	frugivore	Phyllostomidae	155.087108
<i>Chironax melanocephalus</i>	Non	frugivore	Pteropodidae	136.055402
<i>Choeronycteris mexicana</i>	Nasal	nectarivore	Phyllostomidae	142.719328
<i>Chrotopterus auritus</i>	Nasal	carnivorous	Phyllostomidae	150.032562
<i>Cistugo lesueuri</i>	Oral	insectivore	Cistugidae	124.858301
<i>Coelops frithii</i>	Nasal	insectivore	Hipposideridae	167.211148
<i>Coleura afra</i>	Oral	insectivore	Emballonuridae	142.674458
<i>Cormura brevirostris</i>	Oral	insectivore	Emballonuridae	128.769671
<i>Corynorhinus townsendii</i>	Oral	insectivore	Vespertilionidae	134.011313

<i>Craseonycteris thonglongyai</i>	Oral	insectivore	Craesonycteridae		137.888875
<i>Cynomops abrasus</i>	Oral	insectivore	Molossidae		117.895728
<i>Cynopterus brachyotis</i>	Non	frugivore	Pteropodidae		139.344215
<i>Cynopterus titthaechelilus</i>	Non	frugivore	Pteropodidae		141.619747
<i>Desmodus rotundus</i>	Nasal	sanguivore	Phyllostomidae		134.695147
<i>Diaemus youngi</i>	Nasal	sanguivore	Phyllostomidae		138.342479
<i>Diclidurus scutatus</i>	Oral	insectivore	Emballonuridae		114.969797
<i>Diphylla ecaudata</i>	Nasal	sanguivore	Phyllostomidae		141.972619
<i>Dobsonia moluccensis</i>	Non	frugivore	Pteropodidae		141.473317
<i>Dobsonia praedatrix</i>	Non	frugivore	Pteropodidae		133.170663
<i>Eidolon helvum</i>	Non	frugivore	Pteropodidae		147.824943
<i>Emballonura alecto</i>	Oral	insectivore	Emballonuridae		142.985346
<i>Emballonura monticola</i>	Oral	insectivore	Emballonuridae		137.655427
<i>Eonycteris spelaea</i>	Non	nectarivore	Pteropodidae		149.44616
<i>Epomophorus wahlbergi</i>	Non	frugivore	Pteropodidae		125.803689
<i>Epomops franqueti</i>	Non	frugivore	Pteropodidae		137.444266
<i>Eptesicus fuscus</i>	Oral	insectivore	Vespertilionidae		116.963262
<i>Eptesicus serotinus</i>	Oral	insectivore	Vespertilionidae		116.459472
<i>Eumops auripectus</i>	Oral	insectivore	Molossidae		135.50939
<i>Eumops glaucinus</i>	Oral	insectivore	Molossidae		124.406709
<i>Eumops hansae</i>	Oral	insectivore	Molossidae		131.833142
<i>Eumops underwoodi</i>	Oral	insectivore	Molossidae		124.085635
<i>Furipterus horrens</i>	Oral	insectivore	Furipteridae		118.795021
<i>Glauconycteris argentata</i>	Oral	insectivore	Vespertilionidae		92.9758395
<i>Glauconycteris variegata</i>	Oral	insectivore	Vespertilionidae		98.0930036
<i>Glossophaga soricina</i>	Nasal	nectarivore	Phyllostomidae		141.673008
<i>Hesperoptenus tickelli</i>	Oral	carnivorous	Vespertilionidae	X	106.369247
<i>Hipposideros armiger</i>	Nasal	insectivore	Hipposideridae		165.044886
<i>Hipposideros caffer</i>	Nasal	insectivore	Hipposideridae		163.781269
<i>Hipposideros commersoni</i>	Nasal	insectivore	Hipposideridae		153.292747
<i>Hipposideros fulvus</i>	Nasal	insectivore	Hipposideridae		167.369199
<i>Hipposideros pratti</i>	Nasal	insectivore	Hipposideridae		158.39633
<i>Hipposideros speoris</i>	Nasal	insectivore	Hipposideridae		160.53032
<i>Hylonycteris underwoodi</i>	Nasal	nectarivore	Phyllostomidae		140.096941
<i>Hypsignathus monstrosus</i>	Non	frugivore	Pteropodidae		137.676526
<i>Hypsugo crassulus</i>	Oral	insectivore	Vespertilionidae		123.690178
<i>Hypsugo savii</i>	Oral	insectivore	Vespertilionidae	X	110.573404

<i>Idionycteris phyllotis</i>	Oral	insectivore	Vespertilionidae	X	137.717584
<i>Kerivoula minuta</i>	Oral	insectivore	Vespertilionidae		122.956229
<i>Kerivoula pellucida</i>	Oral	insectivore	Vespertilionidae	X	123.486595
<i>Lasionycteris noctivagans</i>	Oral	insectivore	Vespertilionidae		112.016327
<i>Lasiurus blossevillii</i>	Oral	insectivore	Vespertilionidae	X	90.5776057
<i>Lasiurus borealis</i>	Oral	insectivore	Vespertilionidae	X	103.064782
<i>Lasiurus cinereus</i>	Oral	insectivore	Vespertilionidae		93.0718652
<i>Lasiurus ega</i>	Oral	insectivore	Vespertilionidae	X	99.4020861
<i>Lasiurus intermedius</i>	Oral	insectivore	Vespertilionidae		102.846559
<i>Lasiurus seminolus</i>	Oral	insectivore	Vespertilionidae	X	97.3324813
<i>Leptonycteris curasoae</i>	Nasal	nectarivore	Phyllostomidae		132.463348
<i>Lonchophylla robusta</i>	Nasal	nectarivore	Phyllostomidae		140.290603
<i>Lophostoma brasiliense</i>	Nasal	omnivore	Phyllostomidae		149.458576
<i>Lophostoma silvicolum</i>	Nasal	omnivore	Phyllostomidae		151.269489
<i>Macroderma gigas</i>	Nasal	carnivorous	Megadermatidae		144.53627
<i>Macroglossus sobrinus</i>	Non	nectarivore	Pteropodidae		150.145454
<i>Macrophyllum macrophyllum</i>	Nasal	insectivore	Phyllostomidae		143.285138
<i>Macrotus waterhousii</i>	Nasal	insectivore	Phyllostomidae		152.045647
<i>Megaderma spasma</i>	Nasal	insectivore	Megadermatidae		154.107003
<i>Megaerops wetmorei</i>	Non	frugivore	Pteropodidae		135.610642
<i>Mesophylla macconnelli</i>	Nasal	frugivore	Phyllostomidae		158.043275
<i>Micronycteris hirsuta</i>	Nasal	insectivore	Phyllostomidae		153.900329
<i>Micronycteris megalotis</i>	Nasal	insectivore	Phyllostomidae		156.462346
<i>Micronycteris minuta</i>	Nasal	insectivore	Phyllostomidae		149.374324
<i>Micropteropus pusillus</i>	Non	nectarivore	Pteropodidae		141.24158
<i>Mimon crenulatum</i>	Nasal	insectivore	Phyllostomidae		150.750954
<i>Miniopterus australis</i>	Oral	insectivore	Miniopteridae		118.422475
<i>Miniopterus inflatus</i>	Oral	insectivore	Miniopteridae		120.803343
<i>Miniopterus schreibersii</i>	Oral	insectivore	Miniopteridae		114.36929
<i>Molossops temminckii</i>	Oral	insectivore	Molossidae		115.693382
<i>Molossus molossus</i>	Oral	insectivore	Molossidae		142.612175
<i>Molossus rufus</i>	Oral	insectivore	Molossidae		141.99245
<i>Mops condylurus</i>	Oral	insectivore	Molossidae		129.60886
<i>Mormoops blainvillii</i>	Oral	insectivore	Mormoopidae		75.1023756
<i>Mormoops megalophylla</i>	Oral	insectivore	Mormoopidae		75.0662528
<i>Mormopterus planiceps</i>	Oral	insectivore	Molossidae		130.582077
<i>Mosia nigrescens</i>	Oral	insectivore	Emballonuridae		140.515214

<i>Murina aurata</i>	Oral	insectivore	Vespertilionidae	X	139.118145
<i>Murina cyclotis</i>	Oral	insectivore	Vespertilionidae	X	138.452005
<i>Murina huttoni</i>	Oral	insectivore	Vespertilionidae	X	132.823441
<i>Murina leucogaster</i>	Oral	insectivore	Vespertilionidae		131.628323
<i>Myonycteris angolensis</i>	Non	frugivore	Pteropodidae		136.797745
<i>Myonycteris relicta</i>	Non	frugivore	Pteropodidae		141.297358
<i>Myotis capaccinii</i>	Oral	carnivorous	Vespertilionidae		130.914014
<i>Myotis daubentonii</i>	Oral	insectivore	Vespertilionidae		125.766897
<i>Myotis emarginatus</i>	Oral	insectivore	Vespertilionidae		127.091103
<i>Myotis evotis</i>	Oral	insectivore	Vespertilionidae		130.589435
<i>Myotis keenii</i>	Oral	insectivore	Vespertilionidae		125.945374
<i>Myotis lucifugus</i>	Oral	insectivore	Vespertilionidae		125.113295
<i>Myotis myotis</i>	Oral	insectivore	Vespertilionidae		130.379306
<i>Myotis nigricans</i>	Oral	insectivore	Vespertilionidae		123.80648
<i>Myotis simus</i>	Oral	insectivore	Vespertilionidae		121.957735
<i>Myotis sodalis</i>	Oral	insectivore	Vespertilionidae		120.495145
<i>Myotis velifer</i>	Oral	insectivore	Vespertilionidae		124.544797
<i>Myotis yumanensis</i>	Oral	insectivore	Vespertilionidae		123.818722
<i>Mystacina tuberculata</i>	Oral	insectivore	Mystacinidae		134.943649
<i>Myzopoda aurita</i>	Oral	insectivore	Myzopodidae		114.348991
<i>Myzopoda schliemanni</i>	Oral	insectivore	Myzopodidae		113.308271
<i>Natalus stramineus</i>	Oral	insectivore	Natalidae		140.612223
<i>Neoromicia capensis</i>	Oral	insectivore	Vespertilionidae		121.042992
<i>Neoromicia nanus</i>	Oral	insectivore	Vespertilionidae		123.92315
<i>Noctilio albiventris</i>	Oral	insectivore	Noctilionidae		119.819774
<i>Noctilio leporinus</i>	Oral	carnivorous	Noctilionidae		120.057273
<i>Nyctalus leisleri</i>	Oral	insectivore	Vespertilionidae	X	98.0184055
<i>Nyctalus noctula</i>	Oral	insectivore	Vespertilionidae		105.012526
<i>Nyctalus plancyi</i>	Oral	insectivore	Vespertilionidae	X	91.6830459
<i>Nycteris arge</i>	Nasal	insectivore	Nycteridae		170.908211
<i>Nycteris hispida</i>	Nasal	insectivore	Nycteridae		175.125583
<i>Nycteris thebaica</i>	Nasal	insectivore	Nycteridae		168.431952
<i>Nycteris tragata</i>	Nasal	insectivore	Nycteridae		166.445551
<i>Nycticeinops schlieffeni</i>	Oral	insectivore	Vespertilionidae		121.576882
<i>Nycticeius humeralis</i>	Oral	insectivore	Vespertilionidae		120.025256
<i>Nyctimene albiventer</i>	Non	frugivore	Pteropodidae		143.1653
<i>Nyctinomops laticaudatus</i>	Oral	insectivore	Molossidae		131.048689
<i>Nyctinomops macrotis</i>	Oral	insectivore	Molossidae		140.358578
<i>Nyctophilus arnhemensis</i>	Oral	insectivore	Vespertilionidae		135.808132

<i>Otomops martiensseni</i>	Oral	insectivore	Molossidae		139.124518
<i>Paranyctimene raptor</i>	Non	frugivore	Pteropodidae		139.601954
<i>Parastrellus hesperus</i>	Oral	insectivore	Vespertilionidae		115.687788
<i>Penthetor lucasi</i>	Non	frugivore	Pteropodidae		141.208096
<i>Peropteryx kappleri</i>	Oral	insectivore	Emballonuridae		144.977265
<i>Peropteryx trinitatis</i>	Oral	insectivore	Emballonuridae		144.852005
<i>Phylloderma stenops</i>	Nasal	omnivore	Phyllostomidae		151.826476
<i>Phyllostomus discolor</i>	Nasal	omnivore	Phyllostomidae		152.684725
<i>Phyllostomus elongatus</i>	Nasal	omnivore	Phyllostomidae		151.97256
<i>Phyllostomus hastatus</i>	Nasal	carnivorous	Phyllostomidae		149.540063
<i>Pipistrellus coromandra</i>	Oral	insectivore	Vespertilionidae	X	121.508666
<i>Pipistrellus javanicus</i>	Oral	insectivore	Vespertilionidae	X	114.148859
<i>Pipistrellus nathusii</i>	Oral	insectivore	Vespertilionidae	X	124.01636
<i>Pipistrellus pipistrellus</i>	Oral	insectivore	Vespertilionidae	X	117.991541
<i>Pipistrellus subflavus</i>	Oral	insectivore	Vespertilionidae		125.50616
<i>Pipistrellus tenuis</i>	Oral	insectivore	Vespertilionidae	X	122.407751
<i>Platyrrhinus dorsalis</i>	Nasal	frugivore	Phyllostomidae		157.721417
<i>Plecotus auritus</i>	Oral	insectivore	Vespertilionidae		141.747639
<i>Ptenochirus jagori</i>	Non	frugivore	Pteropodidae		157.594595
<i>Pteronotus davyi</i>	Oral	insectivore	Mormoopidae		115.884266
<i>Pteronotus parnellii</i>	Oral	insectivore	Mormoopidae		123.162369
<i>Pteropus poliocephalus</i>	Non	frugivore	Pteropodidae		136.867863
<i>Pteropus scapulatus</i>	Non	frugivore	Pteropodidae		143.932906
<i>Pteropus vampyrus</i>	Non	frugivore	Pteropodidae		118.124734
<i>Rhinolophus acuminatus</i>	Nasal	insectivore	Rhinolophidae		170.093256
<i>Rhinolophus affinis</i>	Nasal	insectivore	Rhinolophidae		181.039423
<i>Rhinolophus blasii</i>	Nasal	insectivore	Rhinolophidae		159.52923
<i>Rhinolophus celebensis</i>	Nasal	insectivore	Rhinolophidae		173.143108
<i>Rhinolophus clivosus</i>	Nasal	insectivore	Rhinolophidae		165.106804
<i>Rhinolophus creaghi</i>	Nasal	insectivore	Rhinolophidae		170.22011
<i>Rhinolophus darlingi</i>	Nasal	insectivore	Rhinolophidae		168.50952
<i>Rhinolophus eloquens</i>	Nasal	insectivore	Rhinolophidae		167.757665
<i>Rhinolophus euryale</i>	Nasal	insectivore	Rhinolophidae		165.416697
<i>Rhinolophus ferrumequinum</i>	Nasal	insectivore	Rhinolophidae		164.542503
<i>Rhinolophus fumigatus</i>	Nasal	insectivore	Rhinolophidae		164.856065
<i>Rhinolophus hildebrandti</i>	Nasal	insectivore	Rhinolophidae		164.066657
<i>Rhinolophus hipposideros</i>	Nasal	insectivore	Rhinolophidae		167.98157

<i>Rhinolophus landeri</i>	Nasal	insectivore	Rhinolophidae		169.537359
<i>Rhinolophus lepidus</i>	Nasal	insectivore	Rhinolophidae		162.295424
<i>Rhinolophus luctus</i>	Nasal	insectivore	Rhinolophidae		175.331309
<i>Rhinolophus macrotis</i>	Nasal	insectivore	Rhinolophidae		169.52486
<i>Rhinolophus mehelyi</i>	Nasal	insectivore	Rhinolophidae		161.606009
<i>Rhinolophus monoceros</i>	Nasal	insectivore	Rhinolophidae		169.821921
<i>Rhinolophus philippinensis</i>	Nasal	insectivore	Rhinolophidae		186.656707
<i>Rhinolophus pusillus</i>	Nasal	insectivore	Rhinolophidae		169.789739
<i>Rhinolophus rex</i>	Nasal	insectivore	Rhinolophidae		163.488741
<i>Rhinolophus rufus</i>	Nasal	insectivore	Rhinolophidae		162.625962
<i>Rhinolophus sedulus</i>	Nasal	insectivore	Rhinolophidae		171.017046
<i>Rhinolophus simulator</i>	Nasal	insectivore	Rhinolophidae		174.387791
<i>Rhinolophus sinicus</i>	Nasal	insectivore	Rhinolophidae		167.134331
<i>Rhinolophus swinnyi</i>	Nasal	insectivore	Rhinolophidae		167.503575
<i>Rhinolophus thomasi</i>	Nasal	insectivore	Rhinolophidae		178.236679
<i>Rhinolophus trifoliatu</i>	Nasal	insectivore	Rhinolophidae		173.137693
<i>Rhinonicteris aurantia</i>	Nasal	insectivore	Hipposideridae		156.540964
<i>Rhinophylla pumilio</i>	Nasal	frugivore	Phyllostomidae		148.90781
<i>Rhinopoma hardwickii</i>	Nasal	insectivore	Rhinopomatidae		141.52194
<i>Rhinopoma muscatellum</i>	Nasal	insectivore	Rhinopomatidae		149.048214
<i>Rhogeessa aeneus</i>	Oral	insectivore	Vespertilionidae	X	118.141413
<i>Rhogeessa parvula</i>	Oral	insectivore	Vespertilionidae		119.71486
<i>Rhogeessa tumida</i>	Oral	insectivore	Vespertilionidae	X	124.067282
<i>Rhynchonycteris naso</i>	Oral	insectivore	Emballonuridae		134.524848
<i>Rousettus aegyptiacus</i>	Non	frugivore	Pteropodidae		147.650453
<i>Rousettus amplexicaudatus</i>	Non	frugivore	Pteropodidae		144.013109
<i>Rousettus leschenaultii</i>	Non	frugivore	Pteropodidae		143.688443
<i>Saccolaimus flaviventris</i>	Oral	insectivore	Emballonuridae		114.127979
<i>Saccopteryx bilineata</i>	Oral	insectivore	Emballonuridae		145.75539
<i>Saccopteryx gymnura</i>	Oral	insectivore	Emballonuridae		147.732112
<i>Saccopteryx leptura</i>	Oral	insectivore	Emballonuridae		143.438479
<i>Sauromys petrophilus</i>	Oral	insectivore	Molossidae		119.59444
<i>Scotoecus hirundo</i>	Oral	insectivore	Vespertilionidae		110.724907
<i>Scotophilus dinganii</i>	Oral	insectivore	Vespertilionidae		104.647801
<i>Scotophilus heathii</i>	Oral	insectivore	Vespertilionidae	X	97.936495
<i>Scotophilus kuhlii</i>	Oral	insectivore	Vespertilionidae		108.201441
<i>Sphaeronycteris toxophyllum</i>	Nasal	frugivore	Phyllostomidae		155.235406

<i>Sturnira lilium</i>	Nasal	frugivore	Phyllostomidae		155.902272
<i>Syconycteris australis</i>	Non	nectarivore	Pteropodidae		151.330007
<i>Tadarida brasiliensis</i>	Oral	insectivore	Molossidae		133.199477
<i>Taphozous hildegardeae</i>	Oral	insectivore	Emballonuridae		113.357489
<i>Taphozous melanopogon</i>	Oral	insectivore	Emballonuridae		122.826474
<i>Thyroptera discifera</i>	Oral	insectivore	Thyropteridae		130.393091
<i>Thyroptera tricolor</i>	Oral	insectivore	Thyropteridae		134.699798
<i>Tonatia saurophila</i>	Nasal	insectivore	Phyllostomidae		157.638147
<i>Trachops cirrhosus</i>	Nasal	carnivorous	Phyllostomidae		136.070841
<i>Triaenops afer</i>	Nasal	insectivore	Hipposideridae		163.637426
<i>Triaenops persicus</i>	Nasal	insectivore	Hipposideridae		165.80988
<i>Tylonycteris pachypus</i>	Oral	insectivore	Vespertilionidae	X	115.214029
<i>Tylonycteris robustula</i>	Oral	insectivore	Vespertilionidae		117.614718
<i>Uroderma bilobatum</i>	Nasal	frugivore	Phyllostomidae		152.672242
<i>Vampyressa pusilla</i>	Nasal	frugivore	Phyllostomidae		156.530427
<i>Vampyrum spectrum</i>	Nasal	carnivorous	Phyllostomidae		139.567794
<i>Vespertilio murinus</i>	Oral	insectivore	Vespertilionidae	X	123.30261